NeuroImage 300 (2024) 120835

Contents lists available at ScienceDirect

NeuroImage

journal homepage: www.elsevier.com/locate/ynimg

The strength of anticipated distractors shapes EEG alpha and theta oscillations in a Working Memory task

Elisa Magosso [a,b,*], Davide Borra [a]

[a] Department of Electrical, Electronic and Information Engineering "Guglielmo Marconi" (DEI), University of Bologna, Cesena Campus, Cesena, 47521, Italy
[b] Alma Mater Research Institute for Human-Centered Artificial Intelligence, University of Bologna, Bologna, 40126, Italy

ARTICLE INFO

Keywords:
Event-related spectral perturbation
Visual Sternberg task
Spectral Granger causality
Encoding and retention
Top-down and bottom-up influences
Enhancement and suppression

ABSTRACT

Working Memory (WM) requires maintenance of task-relevant information and suppression of task-irrelevant/distracting information. Alpha and theta oscillations have been extensively investigated in relation to WM. However, studies that examine both theta and alpha bands in relation to distractors, encompassing not only power modulation but also connectivity modulation, remain scarce. Here, we depicted, at the EEG-source level, the increase in power and connectivity in theta and alpha bands induced by strong relative to weak distractors during a visual Sternberg-like WM task involving the encoding of verbal items. During retention, a strong or weak distractor was presented, predictable in time and nature. Analysis focused on the encoding and retention phases before distractor presentation. Theta and alpha power were computed in cortical regions of interest, and connectivity networks estimated via spectral Granger causality and synthetized using in/out degree indices. The following modulations were observed for strong vs. weak distractors. In theta band during encoding, the power in frontal regions increased, together with frontal-to-frontal and bottom-up occipital-to-temporal-to-frontal connectivity; even during retention, bottom-up theta connectivity increased. In alpha band during retention, but not during encoding, the power in temporal-occipital regions increased, together with top-down frontal-to-occipital and temporal-to-occipital connectivity. From our results, we postulate a proactive cooperation between theta and alpha mechanisms: the first would mediate enhancement of target representation both during encoding and retention, and the second would mediate increased inhibition of sensory areas during retention only, to suppress the processing of imminent distractor without interfering with the processing of ongoing target stimulus during encoding.

1. Introduction

Working memory (WM) is the ability to actively store and/or manipulate mental representations, at the ready for immediate use (Postle, 2006), and it is a key component of a wide range of high-level cognitive functions such as learning, problem-solving, decision-making, language comprehension. The operational stages of WM include an encoding phase for loading information in memory, a retention phase for maintenance of the memory trace, and a retrieval phase for information recovery and use. Several WM tasks are used in the literature. In some of them, the WM stages occur in parallel, such as in n-back tasks, while in others the WM stages are temporally segregated, as in Sternberg-like tasks. Common essential elements of WM are the selection of task-relevant information and the inhibition of irrelevant or distracting information. To enhance this selective processing, WM studies often involve manipulation of task-relevant and/or task-irrelevant/distracting information.

A large body of electroencephalogram (EEG) and magnetoencephalogram (MEG) studies points to the strong involvement of brain oscillations in WM processes. Although both beta (13–30 Hz) and gamma (>30 Hz) rhythms have also been investigated in relation to WM (Hwang et al., 2005; Koshy et al., 2020; Proskovec et al., 2019; Schmidt et al., 2019), the majority of the literature in the field focused on theta band (4–7 Hz) and alpha band (8–12 Hz). Despite the extensive body of research on these two rhythms, investigations that jointly examine both theta and alpha band, encompassing not only power modulation but also connectivity modulation, remain scarce, particularly in relation to distractor protection. Further examination of these aspects may yield

* Corresponding Author. Elisa Magosso, Department of Electrical, Electronic and Information Engineering "Guglielmo Marconi", University of Bologna – Cesena Campus, Via dell'Università 50,47521 Cesena (FC) Italy.
E-mail address: elisa.magosso@unibo.it (E. Magosso).

https://doi.org/10.1016/j.neuroimage.2024.120835
Received 26 February 2024; Received in revised form 10 August 2024; Accepted 3 September 2024
Available online 7 September 2024

additional insights into the brain mechanisms and subprocesses that support WM functions. In the following, the key findings about theta and alpha rhythms are reviewed, and the existing gaps that have prompted the present investigation are stressed.

1.1. Theta and alpha oscillations in WM tasks

Theta activity was found to consistently increase during WM (see for review Hsieh and Ranganath, 2014; Klimesch, 1999; Pavlov and Kotchoubey, 2022; Sauseng et al., 2010). For example, enhanced theta power across multiple areas (frontal, temporal and posterior) was obtained in an intracranial EEG study during the encoding and retention of visually presented verbal information (Raghavachari et al., 2001), and in other non-invasive EEG studies during the encoding of lexical, visuo-spatial, and audio-visual information (Jaiswal et al., 2010; Sederberg et al., 2003; Xie et al., 2021). Moreover, theta activity, especially in the frontal midline region, was observed to be positively correlated with the WM load, i.e., the amount of relevant information to be remembered (Jensen and Tesche, 2002; Meltzer et al., 2008; Onton et al., 2005; Proskovec et al., 2019; Scheeringa et al., 2009). Also, an increase in theta connectivity was reported between frontal and temporo-parietal regions during information retention (Sarnthein et al., 1998) and encoding (Kustermann et al., 2018; Sauseng et al., 2004), even exhibiting a positive correlation with the WM load (Kustermann et al., 2018). Theta oscillations in WM have been associated with different mechanisms, possibly coexisting and acting in parallel (see for review Hsieh and Ranganath, 2014; Sauseng et al., 2010); a general mechanism of mental effort and executive control, common to cognitive-demanding tasks and mainly related to midfrontal theta activity (see also Cavanagh and Frank, 2014); a more memory-specific mechanism, according to which theta oscillations across distributed brain areas would coordinate the activation of different item representations (each locked to a different phase of the theta cycle). While previous studies manipulated the relevant items (targets), only a few studies considered theta activity in relation to both distractors and targets (de Vries et al., 2019; Riddle et al., 2020). These studies reported increased midfrontal theta power associated with ignoring distractors (de Vries et al., 2019), possible reflecting executive control increase, and suggested a role of theta activity in prioritizing relevant representations over irrelevant ones (Riddle et al., 2020).

As to alpha-band oscillations, the general view is that they have a role in modulating cortical excitability. Alpha suppression is thought to reflect an increase in neuronal excitability (or a release of inhibition), while alpha enhancement reflects decreased excitability (or increase in inhibition). Thus, alpha activity is considered a mechanism able to flexibly inhibit brain activities not involved in the task at hand, to protect task-relevant processes from possible intrusions (de Vries et al., 2020; Frey et al., 2015; Jensen and Mazaheri, 2010). In the WM context, alpha-band activity has been mainly investigated during retention, showing an increase especially (but not only) in occipital regions, stronger for successfully remembered stimuli compared to forgotten stimuli (Khader et al., 2010), and positively correlated to memory load and task demand (Jensen et al., 2002; Klimesch et al., 1999; Proskovec et al., 2019; Scheeringa et al., 2009). These alpha effects have been interpreted as reflecting disengagement of sensory areas to suppress visual stream input that could disturb the maintenance of the encoded representations. This interpretation is reinforced by results of other WM studies (Jokisch and Jensen, 2007; Sauseng et al., 2009; Vissers et al., 2016) that instructed or cued the subject about which items, displayed during the encoding phase, have to be remembered (task-relevant items) or ignored (task-irrelevant or distractors): during retention, more alpha power increase was observed over the brain regions devoted to the processing of irrelevant items, and it was associated with the suppression of representation of the disturbing information. One of these studies (Vissers et al., 2016) also showed that alpha modulation was present not only during retention (i.e., after items appearance) but developed before items appearance once the cue was provided, thus supporting a preparatory role of alpha oscillations in expectancy of distracting and/or target information. This is in line with other studies, outside the WM context, that involve attentional cuing tasks and report post-cue alpha power increase before stimuli presentation, selectively over brain regions where potential distractors would be processed (e.g., see Doesburg et al., 2016; Fu et al., 2001; Snyder and Foxe, 2010). In WM, other studies show alpha power modulation prior to expected distractors (see Noonan et al., 2018 for review). For example, in Payne et al. (2013), two Gabor patches were serially presented to participants, who were pre-cued about the patch to be remembered and ignored: the to-be-ignored patch was preceded and accompanied by greater alpha power. In a Sternberg-like task, distractors were displayed during the retention interval, with presentation onset predictable in time: parieto-occipital alpha power was found to increase in advance of distractor appearance (Sghirripa et al., 2021). According to a prevailing model, alpha power modulation in posterior sensory cortices, as observed in the previous studies, is affected by top-down influences from frontal and parietal areas via long-range connections (Foxe and Snyder, 2011; Noonan et al., 2018). This hypothesis is substantiated by works providing directed measures of inter-regional functional connectivity during attentional cueing tasks and WM tasks (e.g., Doesburg et al., 2016; Sauseng et al., 2005; Wang et al., 2016).

1.2. Motivation of the present study

Despite the extensive research, some aspects are still overlooked and may benefit from additional investigations.

First, while variations in memory load or demand have been widely investigated, only a few studies considered the load or strength of the distractors and their influence on oscillatory dynamics (the distractor strength representing the degree of similarity between distractors and relevant items). Moreover, these studies report contradictory results. For instance (but see also (Sauseng et al., 2009; Vissers et al., 2016) for contradictory effects of distractor load), Bonnefond and Jensen (2012) investigated the effects of predictable distractors with different strengths (weak and strong) presented in the retention phase of a Sternberg task, obtaining that the anticipation of strong vs. weak distractors was accompanied by greater occipital alpha power before the distractor onset. In a similar task by Sghirripa et al. (2021), no difference in anticipatory alpha power was obtained across the two distractor conditions. Performing additional studies may enrich the description of alpha modulation by distractor strength, possibly also interpreting previous discrepancies.

Second, theta activity has been scarcely explored in relation to distractors and their strength. To the best of our knowledge, only one study (Fodor et al., 2020) examined theta in addition to alpha oscillations in a Stenberg-like task using two types of non-predictable distractors (weak and strong) presented during retention, but only the reaction to distractors was considered and not the preparation for predictable distractors. Since theta rhythm is known to have an important role even during the encoding phase, it would be of high relevance to explore theta activity modulations during the encoding of the memory set, when different types of distractors that will interfere during retention can be anticipated.

Third, several studies have investigated brain connectivity that emerges during WM processes, both in alpha band and theta band (e.g., Kustermann et al., 2018; Sauseng et al., 2005, 2004; Wianda and Ross, 2019), also taking advantage of graph theory indices to characterize the topological properties of the emerging connectivity patterns (Dai et al., 2017; Toppi et al., 2017). However, we are not aware of any study that investigates the impact of different types of distractors (e.g., weak vs. strong) on theta and alpha connectivity patterns. Due to the importance of brain connectivity in implementing cognitive tasks, an approach that goes beyond the analysis of local oscillatory power and considers interregional communications, has the potential to improve the

characterization of the neural mechanisms that operate to handle different types of distractors in WM processing.

The aim of the present study is to contribute to these so far under-explored aspects, also in view of the prospective implications that may derive from a better elucidation of how WM 'resists' to distractors. Indeed, distraction resistance is recognized as a key factor for WM functions and a main determinant of WM capacity. Deterioration of the ability to effectively exclude distraction contributes to WM performance reduction in aging and in psychiatric and neurological disorders, such as attention deficit hyperactivity disorder (ADHD), mild cognitive impairment, and schizophrenia (Anticevic et al., 2012; Aurtenetxe et al., 2016; Lorenc et al., 2021; McNab et al., 2015). A better characterization of the role of brain rhythms in handling distractors in the different phases of WM could improve understanding of the basis of WM impairment in these patients; it could also be relevant for ameliorating WM dysfunctions, by allowing a more informed definition of training protocols (e.g., via transcranial magnetic stimulation and oscillatory entrainment) for possible modulation of the oscillatory patterns during WM tasks.

To the above-mentioned aim, we recorded EEG signals during a Sternberg-like task (as the one used in Sghirripa et al., 2021) where a set of verbal items (letters) was visually presented during the encoding phase. During the retention interval, either a weak distractor (set of symbols) or a strong distractor (set of letters) was displayed, which was predictable in time and nature. EEG sources were then estimated, and we computed alpha (8–12 Hz) and theta (4–7 Hz) power in cortical regions of interest, and inter-regional connectivity via spectral Granger causality, summarized via Graph Theory-derived indices (in degree and out degree centrality indices). We compared, at the source-level, the two distractor conditions in anticipation of distractors, with emphasis on the encoding phase as to theta band and on the retention period before the distractor presentation as to alpha band. In particular, based on existing literature, we were interested in evaluating the increase in theta and alpha activity induced by strong relative to weak distractors. We expected that our approach might reveal different distractor-related increase in cortical power and connectivity patterns, depending on the frequency band and task phase.

2. Materials and methods

2.1. Participants

Twenty-one healthy volunteers (6 males, age 25.3 ± 2.3 years) participated in the study. They had normal or corrected-to-normal vision. Eighteen of them were right-handed. The study was carried out in accordance with the Declaration of Helsinki and approved by the Bioethics Committee of the University of Bologna (protocol number 29146, year 2019); written informed consent was obtained from all participants before the beginning of the experiment. All data were analyzed and reported anonymously.

2.2. Experimental protocol

The protocol consisted of a modified visual Sternberg task; the task was inspired by the one adopted by Sghirripa et al. (2021). The structure of each trial is schematically represented in Fig. 1. Specifically, each trial started with a fixation interval (*rest phase*) randomly lasting between 2 and 2.5 s, during which a central fixation cross was presented on a screen. A randomly selected memory set composed of five unique consonants was then displayed for 2 s and the participant had to memorize it (*encoding phase*). Then, the participant had to maintain the encoded set for 5 s in total (*retention phase*). This phase was in turn composed of an *early retention phase* of 2 s, a *distractor phase* of 1.5 s, and a *late retention phase* of 1.5 s. During the early and late retention phases, the fixation cross was presented on the screen. Conversely, during the distractor phase, a distractor stimulus was presented. This could be a random set of three unique consonants not presented in the memory set (in the following denoted as *strong distractor*), or a set of three symbols "#" (in the following denoted as *weak distractor*). At the end of the retention phase, a probe consonant was presented on the screen, and the participant had to respond whether it belonged or not to the encoded memory set, by pressing the left arrow key or the right arrow key, respectively, with the index and medium fingers. The response provided by the participant ended the current trial and started the following one. The duration of the rest phase, the sequence of consonants defining the memory set and the strong distractor were randomly sampled at each trial. Participants were instructed to minimize eye and limb movements and to answer as accurately as possible to the probe letter. All visual

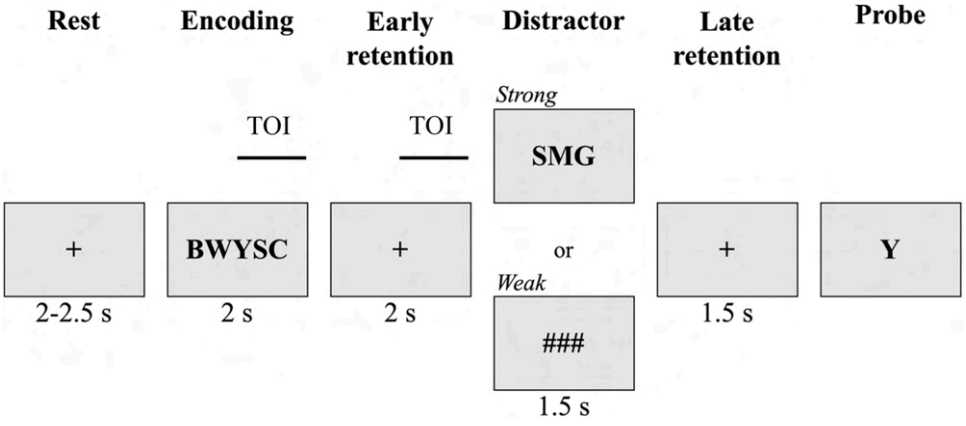

Fig. 1. Modified visual Sternberg task: trial structure. The gray boxes show an example of the visual stimuli presented on the monitor in front of the participant along the phases of the trial. Each trial started with a fixation interval (rest phase). Then, a memory set composed of 5 consonants was displayed (encoding phase) and the participant had to encode it. When the memory set disappeared, the participant had to maintain it in memory (retention phase). This phase was subdivided into three phases: an early retention phase, a distractor phase, and a late retention phase. During the distractor phase, a distractor stimulus (strong: set of 3 consonants, weak: set of 3 equal symbols) was presented. Lastly, a probe consonant was displayed, and the participant had to respond whether it belonged or not to the memory set (probe phase). On top of grey boxes, the two Time intervals Of Interest (TOI) are marked. Event-related spectral perturbations and connectivity at cortical level were analyzed in the encoding TOI (last 1s-length interval of the encoding phase) and in the retention TOI (last 1s-length interval of the early retention phase). See text for further details.

stimuli (fixation cross, memory set, distractors) were shown on a 27inch-screen placed in front of the participant at a distance of approximately 50 cm. The presentation of all visual stimuli was handled by a custom MATLAB script (version R2023a, The Mathworks Inc., Natick, Massachusetts, United States). Keyboard responses were also collected by the custom script for assessing response accuracy and reaction time.

Trials were acquired in 20 separate recording blocks, with a short break between blocks, to reduce participants' fatigue. In each recording block, 20 trials were acquired (400 trials in total). During each block, only one type of distractor (strong or weak) was used, such that participants could anticipate the strength of the distractor within blocks. Importantly, also the onset of the distractor (appearing always 2 seconds after the offset of the memory set) was predictable across trials. Ten recording blocks (200 trials) were recorded for each distractor strength, and the order of the distractor strength was randomly chosen across blocks.

2.3. EEG data acquisition

Each participant wore an EEG cap with 61 electrodes (1 passive ground electrode and 60 active g.SCARABEO electrodes, g.tec Medical Engineering GmbH, Schiedlberg, UA, Austria) placed according to the 10/10 system. The reference electrode was placed on the right earlobe and the ground electrode in AFz. Signals were amplified with a g.HIamp80 RESEARCH amplifier (g.tec Medical Engineering GmbH, Schiedlberg, UA, Austria), sampled at 512 Hz, and electrode impedances were kept below 50 kΩ. A notch digital filter (stopband: 48–52 Hz) was applied during recording.

2.4. Pipeline of EEG data analysis

For each participant, the following EEG pre-processing steps (see Section 2.4.1) and analysis steps (see Sections 2.4.2 to 2.4.5) were conducted.

2.4.1. Pre-processing

The pre-processing consisted of the following offline steps:

i. Linear detrending of signals belonging to each recording block.
ii. Band-pass filtering between 1–60 Hz (IIR elliptic filters; for the low-pass: passband edge frequency =60 Hz, stopband edge frequency = 80 Hz, order = 6; for the high-pass: passband edge frequency = 1 Hz, stopband edge frequency = 0.5 Hz, order = 4; stopband attenuation of at least 40 dB, passband ripple of no more than 0.1 dB) and notch filtering at 50 Hz (second order IIR filter, with notch at 50 Hz and -3 dB bandwidth of 2.2 Hz) of signals belonging to each recording block. Notch filtering was also applied offline since the visualization of the power spectral density of the recorded EEG signals evidenced insufficient attenuation of the power line noise by the filter applied during recording.
iii. Identification of bad channels within each recording block via random sample consensus method (Fischler and Bolles, 1981).
iv. Concatenation of electrode signals across recording blocks.
v. Removal of channels that were labelled as bad (step iii) at least in one recording block, from the concatenated signals. On average, 3 channels (standard deviation, SD = 2) per subject were removed, ranging from 0 to 7.
vi. Removal of artifacts (ocular, muscular, heart and channel noise) via independent component analysis (ICA). ICA was computed using the extended Infomax algorithm (Lee et al., 1999) applied to the concatenated signals (free from bad channels). We visually explored each IC (its time pattern, power spectral density and scalp topological map) and ICs likely having artifact origin were eliminated. On average, 18 ICs (SD = 3.8) per subject were removed, ranging from 10 to 24. This large number of removed ICs derived from the concatenation of all recording blocks, so that the signal subjected to IC decomposition for each participant was very long, overall lasting about 4300 s.
vii. Spherical spline interpolation of the bad channels removed in step v.
viii. Epoching into 5s-length epochs, starting 1 s before and ending 4 s after the presentation of the memory set, i.e., including the last 1s-interval of the rest phase, the encoding phase and the early retention phase (in each epoch, time 0 s corresponded to the onset of the memory set).
ix. Baseline correction of each epoch, by removing the mean value computed over the rest interval from -1 s to 0 s, channel by channel.
x. Common average re-referencing.

The adopted pre-processing pipeline was similar to the one used in our previous study analyzing cortical power and connectivity in a different task (Borra et al., 2023).

In the following, we present the analyses performed at the EEG source level as to event-related spectral perturbation and connectivity. Preliminary analyses at the electrode level did not provide any significant results; therefore they are not presented. However, for completeness, Supplementary Materials (see Section S1-1.1, Figs. S1 and S2) report the time-frequency patterns of event-related spectral perturbations, over the entire frequency range and in theta and alpha band, computed at the electrode level.

2.4.2. EEG source imaging

Sensor-space signals (scalp signals) were transformed into source-space signals (cortical signals) using MNE Python library (version 1.2.2) (Gramfort et al., 2013). To this end, we used the template head anatomy FSaverage, together with the default electrode position distributed with the template head model and already aligned to it. The source space was restricted to the cortex and discretized into 20,484 vertices. The forward problem was solved via the boundary element method with MNE default parameters. The inverse problem was solved using eLORETA (exact Low Resolution Electromagnetic Tomography) (Pascual-Marqui et al., 2011) with MNE default parameters, with an identity noise covariance matrix, and with the dipole source orientation constrained to be perpendicular to the cortex. By doing so, each cortical vertex was associated with one source signal (20,484 signals).

2.4.3. Cortical parcellation: computation of quantities functional for the following analyses at two spatial resolutions

We achieved a first reduction of the dimension of the source space (20,484 time series) to a manageable number of signals by adopting the parcellation of the cortical surface based on one existing atlas, available in MNE Python library, specifically the Desikan-Killiany (DK) atlas (Desikan et al., 2006), which considers 68 parcels (34 per hemisphere), in the following denoted as DK parcels. The list of the 34 DK parcels and of their abbreviations is reported in Table 1 (left column), and their location over the cortex is displayed in Fig. 2. For each trial, a waveform representative of the neural activity of each DK parcel was derived, by averaging all signals of the vertices belonging to that parcel. To avoid cancelling out the neural activity in case of many vertices within the parcel having dipole orientations in opposite directions, the signs of source signals that were not oriented as the "dominant direction" were flipped before averaging (Ghumare et al., 2018). The dominant direction corresponded to the first principal direction of the orientations of the dipoles belonging to the parcel.

From the signals at the DK parcels, we derived event-related spectral perturbations and functional connectivity quantities that served as starting point for the subsequent analyses at two different spatial resolution levels (see Sections 2.4.4 and 2.4.5). Specifically, the following computations were applied to the DK parcels subject by subject.

Table 1
List of the Desikan-Killiany (DK) parcels, together with the ROIs and macro-ROIs used in the analyses. *Left column*: complete name of each DK parcel and the corresponding label (34 parcels per hemisphere). *Middle column*: complete name and label of each ROI (14 ROIs per hemisphere). *Right column:* complete name and label of each macro-ROI, i.e., lobe (3 macro-ROIs per hemisphere). The analyses were performed at the macro-ROI level and at the ROI-level. See text for further explanations.

DK parcels (34 per hemisphere)	ROIs (14 per hemisphere)	Macro-ROIs (3 per hemisphere)
caudal anterior-cingulate cortex (cAC) rostral anterior-cingulate cortex (rAC)	anterior cingulate cortex (AC)	
pars opercularis (pOP) pars orbitalis (pOR) pars triangularis (pTR)	inferior frontal gyrus (IF)	
caudal middle frontal gyrus (cMF) rostral middle frontal gyrus (rMF)	middle frontal gyrus (MF)	frontal (F)
paracentral lobule (PAC)	paracentral lobule (PAC)	
precentral gyrus (PRC)	precentral gyrus (PRC)	
lateral orbital frontal cortex (lOF) medial orbital frontal cortex (mOF)	orbital frontal cortex (OF)	
frontal pole (FP) superior frontal gyrus (SF)	superior frontal gyrus extended (SFe)	
inferior temporal gyrus (IT)	inferior temporal gyrus (IT)	
banks superior temporal sulcus (BK) middle temporal gyrus (MT)	middle temporal gyrus extended (MTe)	
superior temporal gyrus (ST) transverse temporal cortex (TT)	superior temporal gyrus extended (STe)	temporal (T)
entorhinal cortex (EN) fusiform gyrus (FU) parahippocampal gyrus (PH) temporal pole (TP)	medial temporal gyrus (mT)	
lateral occipital cortex (LO)	lateral occipital cortex (LO)	
cuneus cortex (CU) lingual gyrus (LG) pericalcarine cortex (PCL)	medial occipital cortex (mO)	occipital (O)
isthmus-cingulate cortex (IST) posterior-cingulate cortex (PCG)	posterior cingulate cortex (PC)	
inferior parietal cortex (IP) postcentral gyrus (POC) precuneus (PCU) superior parietal cortex (SP) supramarginal gyrus (SMG) insular cortex (IN)		

2.4.3.1. Event-related spectral perturbations. For each 5s-epoch, event-related spectral perturbations (ERSPs) were obtained parcel by parcel as follows. At first, the continuous wavelet transform of the parcel signal was computed using complex Morlet wavelet as basis function. Wavelet transform coefficients were then squared to obtain time-frequency power representations. These representations were normalized using the rest interval between -1 and 0 s as baseline (Grandchamp and Delorme, 2011); specifically we computed the difference between the power at each time-frequency point and the average baseline power at the same frequency (i.e., the mean power value between -1 and 0 s at that frequency), and divided the result by the same average baseline power. Then, the ERSP was obtained by averaging the normalized representations across epochs, separately for strong and weak distractor conditions. The ERSP was averaged over the theta band (4–7 Hz) and alpha band (8–12 Hz), obtaining *theta-ERSP* and *alpha-ERSP* for each parcel as a function of time during the epoch from –1 s to 4 s, separately for strong and weak distractor conditions.

Then, for each parcel, we considered theta- and alpha-ERSP within a specific Time-interval Of Interest (TOI), separately for each distractor condition. As the theta rhythm is known to be involved in encoding useful information, and the alpha rhythm in inhibiting interfering information, we focused the analysis of theta-ERSP within the last 1s-length interval of the encoding phase, i.e., from 1 s to 2 s (in the following denoted as *encoding TOI*), and of alpha-ERSP within the last 1s-length interval of the early retention phase, i.e., from 3 s to 4 s (in the following denoted as *retention TOI)*. We considered ERSP within 1s-length TOIs (the last second of both examined phases) in order to eliminate contamination by the evoked potentials elicited by the visual stimuli immediately at the onset of the encoding phase and of the early retention phase (that is, the appearance of the memory set at the onset of the encoding phase and the appearance of the fixation cross at the onset of the early retention phase).

2.4.3.2. Connectivity matrices. We estimated the directional influences between the DK cortical parcels in the theta band and alpha band by computing pairwise Granger causality (GC) (Granger, 1969) in the frequency domain. By denoting with $x_i[n]$ and $x_j[n]$ two time series, here corresponding to the cortical signals representative of the i-th and j-th parcel, the system $[x_i[n];\ x_j[n]]$ can be represented using a bivariate autoregressive model with order p ($p = 30$ in this study, as we adopted in past studies (Borra et al., 2023; Magosso et al., 2021)). By Fourier-transforming this time-domain representation, a spectral representation is obtained. Then, the power spectrum of each time series (e.g., $x_i[n]$) can be computed according to Geweke (Geweke, 1982) and decomposed into an intrinsic term and a causal term, the latter being the term predicted by the other time series (e.g., $x_j[n]$). The spectral GC from the j-th to the i-th parcel at each frequency f, $GC_{j\to i}(f)$, is defined as the log of the ratio between the total power of $x_i[n]$ at f and the difference between the total power of $x_i[n]$ at f and the causal power exerted by $x_j[n]$ onto $x_i[n]$ at f. Thus, the quantity $GC_{j\to i}(f)$ increases as the causal power increases. At each frequency f, the spectral GC is represented by a non-symmetric matrix with shape $N \times N$ (here $N = 68$), where the off-diagonal ji-th value quantifies the directional influence from the j-th parcel to the i-th parcel at that frequency ($GC_{j\to i}(f)$).

Spectral GC was computed within the same TOIs used for ERSPs, that is within the encoding TOI for the theta band and the retention TOI for the alpha band. We used these TOIs also for the connectivity analysis since the first second of each phase (i.e., from 0 to 1 s and from 2 to 3 s) was influenced by the transient due to the visual event related potential, elicited by the appearance/disappearance of visual stimuli on the screen. Moreover, to compensate for residual non-stationarities that might occur also in the considered time windows, the evoked potential was removed from each epoch before computing the Granger Causality (Wang et al., 2008). For each subject and each distractor strength, the cortical signals within TOIs were concatenated together across epochs, separately for the encoding TOI and the retention TOI. Then, the spectral Granger Causality was computed over the concatenated signals. By doing so, the directional influences between the DK parcels in the spectral domain were estimated separately for the strong and weak distractor conditions and for the encoding and retention TOIs. From the spectral GC obtained in the encoding TOI, theta-band connectivity was computed by averaging the values of the GC spectrum belonging to the theta band, separately in the strong and weak distractor conditions. Similarly, from the spectral GC obtained in the retention TOI, alpha band connectivity was computed by averaging the values of the GC spectrum belonging to the alpha band, separately in the strong and weak distractor conditions. This resulted into 4 connectivity matrices per

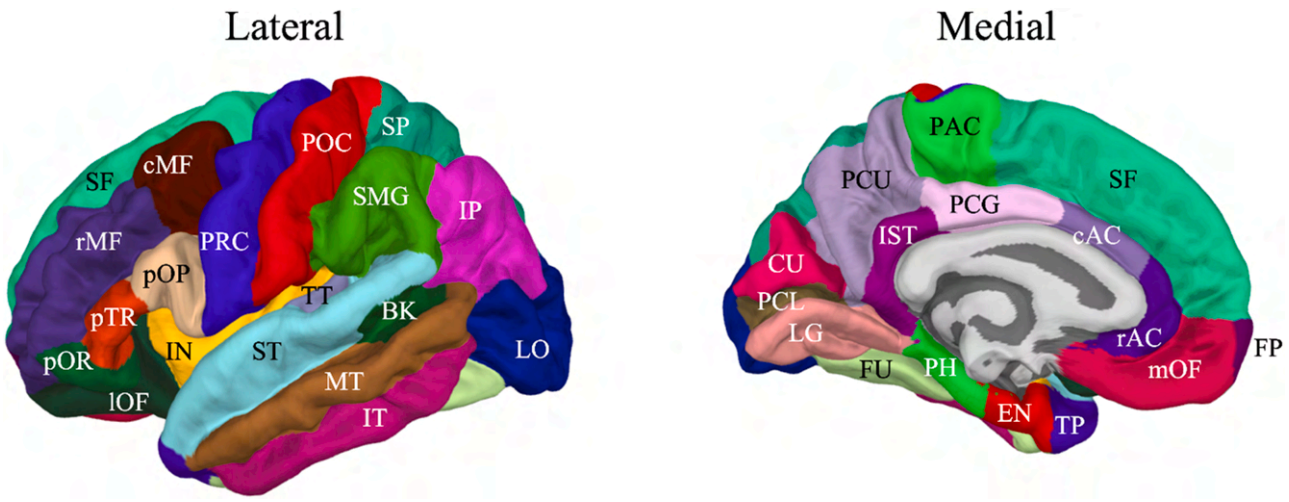

Fig. 2. Location of the DK parcels. The figure shows the cortical surface parcellation according to the Desikan-Killiany (DK) Atlas. Each parcel is labelled by its abbreviation (label) as reported in Table 1 (see left column). Note that the analyses were applied at the macro-ROI level and at the ROI-level, i.e. at lower spatial resolution than the DK parcels.

subject (each of size 68 × 68), denoted as *parcel connectivity matrices*. Each matrix consisted of 68*67 values, since all self-connections were excluded.

2.4.4. Analyses at lobe-level (macro-ROIs, 3 per hemisphere): event-related spectral perturbations, connectivity and centrality indices

Starting from the ERSP and connectivity quantities obtained in the previous section (Section 2.4.3), we initially perform an analysis at coarse spatial resolution, by considering macro-ROIs. Specifically, we defined six *macro-ROIs* (corresponding to lobes), three per hemisphere, by aggregating together the DK parcels belonging to the frontal lobe (F), temporal lobe (T) and occipital lobe (O), in each hemisphere (see the right column in Table 1; e.g. the frontal (F) macro-ROI in each hemisphere was obtained by aggregating the 13 frontal DK parcels listed in the left-column cells in correspondence to the right-column cell). Based on the task at hand, we assumed that these are the main involved lobes, and we neglected the parietal lobes. Event-related spectral perturbations, connectivity, and in degree and outdegree indices were then obtained for the macro-ROIs.

2.4.4.1. Event-related spectral perturbations. For each distractor condition separately (strong and weak), theta-ERSP of each macro-ROI in the encoding TOI was obtained by averaging the theta-ERSP across the DK parcels belonging to the macro-ROI, within the encoding TOI. The same procedure was applied for obtaining alpha-ERSP of each macro-ROI in the retention TOI. Then, for each rhythm and its associated TOI, we computed the maximum value of the ERSP (theta: maximum value within 1–2 s interval, alpha: maximum value within 3–4 s interval), macro-ROI by macro-ROI, obtaining the maximum theta-ERSP in the encoding TOI and maximum alpha-ERSP in the retention TOI, separately for strong and weak distractor conditions (one scalar value per macro-ROI per condition). These latter quantities were subjected to statistical comparison across the two distractor conditions (see Section 2.4.6).

2.4.4.2. Connectivity. Connectivity from a macro-ROI (let's say A) to another macro-ROI (let's say B) was obtained by averaging all the connectivity values that emerged from the DK parcels belonging to the macro-ROI A and targeted the DK parcels belonging to the macro-ROI B. The choice of averaging the connectivity across the parcels to estimate the connectivity at the macro-ROIs is supported by a recent study (Brkić et al., 2023), suggesting that when elements are aggregated together, higher accuracy in connectivity estimate is obtained by first computing the connectivity for all elements to be aggregated and then by applying the average. This procedure was applied for each distractor condition (strong and weak) and for each band (theta in encoding TOI and alpha in retention TOI). This resulted into 4 connectivity matrices per subject (each of size 6 × 6), denoted as *macro-ROI or lobe connectivity matrices*. Each matrix consisted of 6*5 values, since all self-connections were excluded. The lobe connectivity matrices were subjected to statistical comparison across the two distractor conditions (see Section 2.4.6).

2.4.4.3. Centrality indices (in degree and out degree). For each macro-ROI, indices derived from the graph theory were obtained from the 6 × 6 connectivity matrices. For each band and distractor strength, we computed two centrality indices: the in degree – i.e., the sum of connectivity values entering in each macro-ROI (quantifying the overall connectivity inflow) – and the out degree – i.e., the sum of connectivity values departing from each macro-ROI (quantifying the overall connectivity outflow). These indices were subjected to statistical comparison across the two distractor conditions (see Section 2.4.6).

2.4.5. Analyses at ROI-level (14 ROIs per hemisphere): event-related spectral perturbations, connectivity and centrality indices

The analyses at lobe-level were useful to investigate coarse traits of the effects mediated by the distractor strength. Subsequently, we performed an analysis at higher spatial resolution, at the level of 28 ROIs (14 ROIs per hemisphere), still covering the frontal, temporal and occipital lobes. The 14 ROIs per hemisphere were obtained by aggregating adjacent DK parcels ensuring that each ROI contained no less than 150 vertices of the cortical tessellation utilized for the inverse problem solution, thereby identifying a cortical zone rather than small parcels (mean number of vertices across the 28 ROIs = 447, range = 162–780; mean number of vertices across the 68 DK parcels= 275, range = 17–763, with 24 DK parcels having less than 150 vertices). The list of the 14 ROIs per hemisphere is reported in Table 1 (see middle column, e.g., the anterior cingulate (AC) ROI in each hemisphere was obtained by aggregating the two DK parcels listed in the left-column cells in correspondence to the middle-column cell, i.e. the rostral (rAC) and caudal anterior cingulate (cAC) cortices). We adopted a less fine resolution than DK parcels for our analysis, in order to mitigate the effect of spatial blurring and localization inaccuracy in source estimation.

2.4.5.1. Event-related spectral perturbations. The same procedure as for the macro-ROIs was adopted here. Specifically, for each distractor condition separately (strong and weak), theta-ERSP of each ROI in the encoding TOI was obtained by averaging the theta-ERSP across the DK

parcels belonging to the ROI, within the encoding TOI. Alpha-ERSP of each ROI in the retention TOI was obtained similarly. Then, as in the case of the macro-ROIs, for each rhythm and its associated TOI, we computed the maximum value of the ERSP (theta: maximum value within 1–2 s interval, alpha: maximum value within 3–4 s interval), ROI by ROI, obtaining the *maximum theta-ERSP* in the encoding TOI and *maximum alpha-ERSP* in the retention TOI, separately for strong and weak distractor conditions (one scalar value per ROI per condition). These quantities were subjected to statistical comparison across the two distractor conditions (see Section 2.4.6). For completeness, in Supplementary Materials (Section S1-1.2), Figs. S3 and S4 report the ERSP for exemplary frontal and occipital ROIs over the 5s-length epoch in the entire frequency range, and in the theta (theta-ERSP) and alpha band (alpha-ERSP). Moreover, Fig. S5 (Section S1-1.2) shows theta-band ERSP in the encoding TOI and alpha-band ERPS in the retention TOI across the 28 ROIs.

2.4.5.2. Connectivity. As for the macro-ROIs, connectivity from a ROI (let's say A) to another ROI (let's say B) was obtained by averaging all the connectivity values that emerged from the DK parcels belonging to the ROI A and targeted the DK parcels belonging to the ROI B. This procedure, applied for each distractor condition (strong and weak) and for each band (theta in encoding TOI and alpha in retention TOI), resulted into 4 connectivity matrices per subject (each of size 28×28), denoted as *ROI complete connectivity matrices.* Each matrix consisted of $28*27 = 756$ values, since all self-connections were excluded. Considering the large number of connections, from the ROI complete connectivity matrices we derived the *ROI sparse connectivity matrices* via statistical comparison between strong and weak distractor conditions, to reduce the noise, as we similarly did in previous studies (Tarasi et al., 2021; Ursino et al., 2022). Specifically, for each band, we performed a two-tailed permutation *t*-test (Nichols and Holmes, 2002) on the 756 connections contrasting strong and weak distractor conditions across the participants (see Section 2.4.6). Then, for each participant and for each band we zeroed the entries in the complete connectivity matrices at the positions corresponding to the connections that resulted not significantly different ($p \geq 0.05$) between the two distractor conditions, retaining only the connections significantly different ($p < 0.05$). This way, we obtained the 4 sparse connectivity matrices per participant, one per each distractor condition and band. The sparse matrices were used for computation of centrality indices at ROI-level.

2.4.5.3. Centrality indices (in degree and out degree). For each ROI, the in degree index (sum of entering connectivity values) and out degree index (sum of exiting connectivity values) were obtained for each band and each distractor condition from the corresponding sparse connectivity matrix. These quantities were subjected to statistical comparison across the two distractor conditions (see Section 2.4.6).

2.4.6. Statistical analyses

All performed statistical analyses concerned pair-wise comparisons between strong and weak distractors conditions across the participants. Normality of distribution was tested using the Anderson-Darling test for all variables. Since for each planned comparison, some of the variables resulted in being non-normally distributed, we used non-parametric tests. Significance level was set at 5%. Correction for multiple comparisons, when applied, was performed via the Benjamini–Yekutieli procedure (Benjamini and Yekutieli, 2001). In cases where tests did not survive correction for multiple comparisons, uncorrected results were reported. All tests were accompanied by effect size computation, to characterize the magnitude of the reported effects.

The following statistical analyses were performed.

i. *Analyses of behavioral results* Comparison of reaction time and of response accuracy between the two distractor conditions. A two-tailed Wilcoxon signed-rank test was performed, separately for each metric (reaction time and response accuracy). Effect size was quantified using *r* (the value of the z-statistic returned by the test, divided by the square root of the sample size). These tests were performed to assess whether behavioral differences across the two conditions were in line with those reported in similar studies.

ii. *Lobe-level analyses*

All the tests performed at lobe-level were one-tail (strong > weak) since we were interested in assessing the *increase* in theta and alpha activity induced by strong relative to weak distractors.

a. Comparison of the maximum theta-ERSP in the encoding TOI and maximum alpha-ERSP in the retention TOI between the two distractor conditions, macro-ROI by macro-ROI. For each band (alpha and theta), we applied a one-tail Wilcoxon signed-rank test (strong>weak) to each macro-ROI. Correction for multiple comparisons was computed within each band (6 comparisons, one per macro-ROI). Effect size was quantified using *r*. These tests were performed to evaluate whether any macro-ROI exhibited theta power increase during encoding or alpha power increase during retention for strong vs. weak distractors.

b. Comparison of theta and alpha connectivity matrices of the macro-ROIs between the two distractor conditions. For each band (theta and alpha), we applied a one-tail Wilcoxon signed-rank test (strong>weak) to each connectivity. Correction for multiple comparisons was computed within each band (30 comparisons, one per bivariate directed connectivity, excluding self-connections). Effect size was quantified using *r*. These tests were performed to evaluate whether any connectivity exhibited increase in theta band during encoding or exhibited increase in alpha band during retention for strong vs. weak distractors.

c. Comparison of theta and alpha in/out degrees of the macro-ROIs between the two distractor conditions. For each band (theta and alpha) and centrality index (in degree and out degree), we applied a one-tail Wilcoxon signed-rank test (strong>weak), to each macro-ROI. Correction for multiple comparisons was computed within each band and centrality index (6 comparisons, one per macro-ROI). Effect size was quantified using *r*. These tests were performed to evaluate whether any macro-ROI exhibited in/out degree increase in theta band during encoding or in alpha band during retention for strong vs. weak distractors.

iii. *ROI-level analyses*

a. Comparison of the maximum theta-ERSP in the encoding TOI and maximum alpha-ERSP in the retention TOI between the two distractor conditions, ROI by ROI. For each band (theta and alpha), we applied a one-tail Wilcoxon signed-rank test (strong>weak) to each ROI. Correction for multiple comparisons was computed within each band (28 comparisons, one per ROI). Effect size was quantified using *r*. These tests were performed to evaluate whether any ROI exhibited theta power increase during encoding or alpha power increase during retention for strong vs. weak distractors.

b. Comparison of the complete theta connectivity matrices and alpha connectivity matrices between the two distractor conditions. For each band (theta and alpha), we applied a two-tail permutation t test (5000 permutations) to each connectivity. Effect size was quantified using *Cohen's d*. This test was performed, according to previous studies (Tarasi et al., 2021; Ursino et al., 2022), to remove basal background noise, by eliminating connectivity items in the complete connectivity matrices that are just noisy (not significant), and moving to sparse connectivity matrices. No correction for multiple comparisons was applied since we wanted to keep as many

connections as possible. Indeed, here we were not interested in each specific connectivity value connecting single pairs of ROIs. Rather we used the resulting sparse matrices for computing centrality indices at ROI-level, to draw cues on an average modulation of the connectivity pattern entering/exiting ROIs, induced by the different distractor strength.

c. Comparison of theta and alpha in/out degrees of the ROIs between the two distractor conditions. For each band (theta and alpha) and centrality index (in degree and out degree), we applied a one-tail Wilcoxon signed-rank test (strong>weak) to each ROI. Correction for multiple comparisons was computed within each band and centrality index. Effect size was quantified using *r*. These tests were performed to evaluate whether any ROI exhibited in/out degree increase in theta band during encoding or in alpha band during retention for strong vs. weak distractors.

While here we focused on connectivity in theta band in the encoding TOI, and connectivity in alpha band in the retention TOI, for completeness in the Supplementary Materials (Section S2) we replicated the analyses considering connectivity in theta band in the retention TOI and connectivity in alpha band in the encoding TOI, both at lobe-level and ROI-level. This was useful to also evaluate alterations in connectivity patterns within a given band when shifting from memory encoding to memory retention.

In the following, any macro-ROI or ROI belonging to the left/right hemisphere will be denoted by adding '.L' / '.R' to the corresponding label.

3. Results

3.1. Behavioral results

Top panels in Fig. 3 display the distributions of the reaction time and response accuracy to the probe in case of strong and weak distractors, separately. Bottom panels show the distributions (represented as violin plots) of the difference of these metrics between the two distractor conditions. Strong distractors were associated with a significant increase in reaction times compared to weak distractors ($m_{S\text{-}W}$ = 0.028 s, $SD_{S\text{-}W}$ = 0.04 s, p = 0.005, r = 0.61). $m_{S\text{-}W}$ represents the mean across subjects of the difference between the quantity in strong distractor condition and in weak distractor condition, and $SD_{S\text{-}W}$ the standard deviation. The response accuracy did not show a significant change across the distractor conditions, although it tended to be slightly lower for strong vs. weak distractors ($m_{S\text{-}W}$ = -0.78%, $SD_{S\text{-}W}$ = -2%, p = 0.1148). These behavioral data are in line with those observed in previous studies in similar task conditions (Bonnefond and Jensen, 2012; Sghirripa et al., 2021).

In the following, first we presented results at lobe-level, both as to ERSP and connectivity, and then at ROI-level. In investigating modulation of connectivity patterns by distractor strength, we were interested in bottom-up connectivity patterns, i.e., along the direction from occipital to temporal to frontal, and in top-down connectivity patterns, i.e., along the direction from frontal to temporal to occipital.

3.2. Lobe-level analyses

Fig. 4 shows the results of the lobe-level analyses as to the theta band during the encoding TOI. Theta ERSP showed a distributed increase of theta activity, involving all considered lobes (occipital, temporal, frontal) but clearly peaking at frontal lobes, both in strong and weak distractor conditions (left and middle columns in Fig. 4a). Comparison between strong and weak distractor conditions revealed larger theta-ERSP in right and left frontal lobes (F.R, F.L) close to significance (right column Fig. 4a, F.L: $m_{S\text{-}W}$ = 0.17, $SD_{S\text{-}W}$ = 0.4, p = 0.0555, r = 0.35; F.R: $m_{S\text{-}W}$ = 0.13, $SD_{S\text{-}W}$ = 0.45, p = 0.0597, r = 0.34; uncorrected p-values). Moreover, strong vs. weak distractors were associated with increased bottom-up occipital-to-temporal connectivity in the left hemisphere (Fig. 4b, $m_{S\text{-}W}$ = 0.002, $SD_{S\text{-}W}$ = 0.0071, p = 0.0143, r = 0.48; uncorrected p-value). This suggests that anticipation of strong vs. weak distractor boosted the engagement of two theta-organized systems, with one working locally at frontal cortices and one working in a bottom-up fashion. In degree and out degree indices of the macro-ROIs showed no difference in the theta band during encoding.

Results concerning the alpha band during retention are presented in Fig. 5. Alpha-ERSP showed a distributed increase of alpha activity too, but assuming largest value at the occipital lobes with a right lateralization, both in strong and weak distractor conditions (left and middle

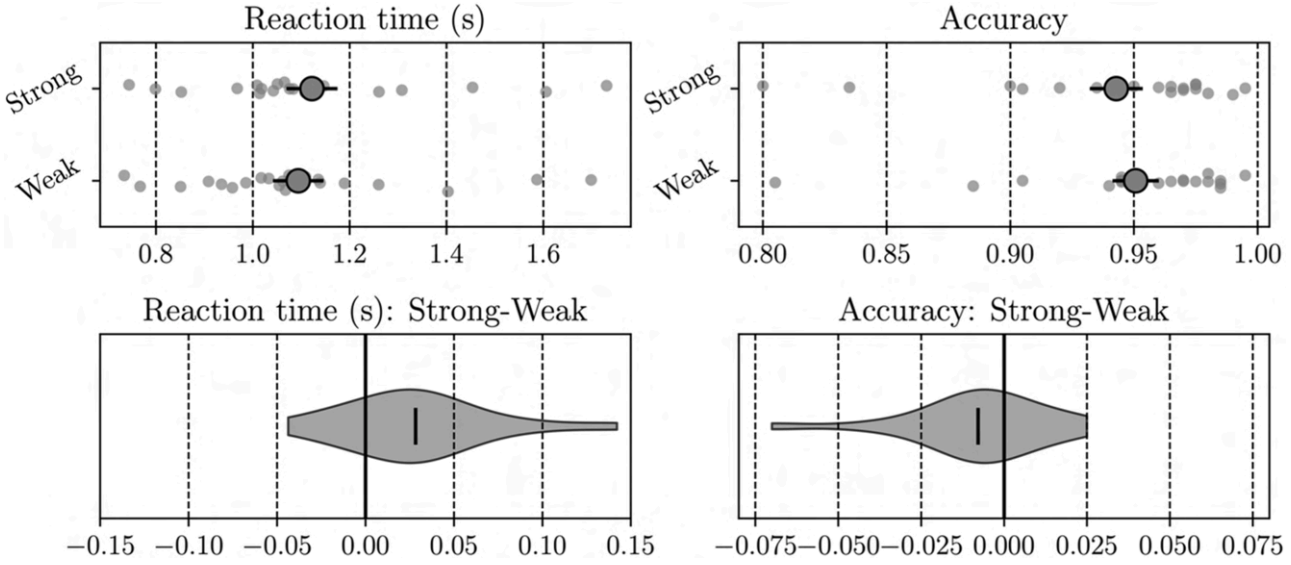

Fig. 3. Reaction time and response accuracy obtained with different distractor strength (strong vs. weak). Reaction time and response accuracy distributions are displayed, separately for strong and weak distractor conditions (top panels). Smaller dots represent the metrics for each subject; bigger dots and black horizontal lines represent the mean value and the standard error of the mean across subjects. The distributions of the difference of the reaction time and response accuracy between strong and weak distractor conditions are reported too (bottom panels), represented as violin plots, with the vertical black line inside each violin plot denoting the mean value.

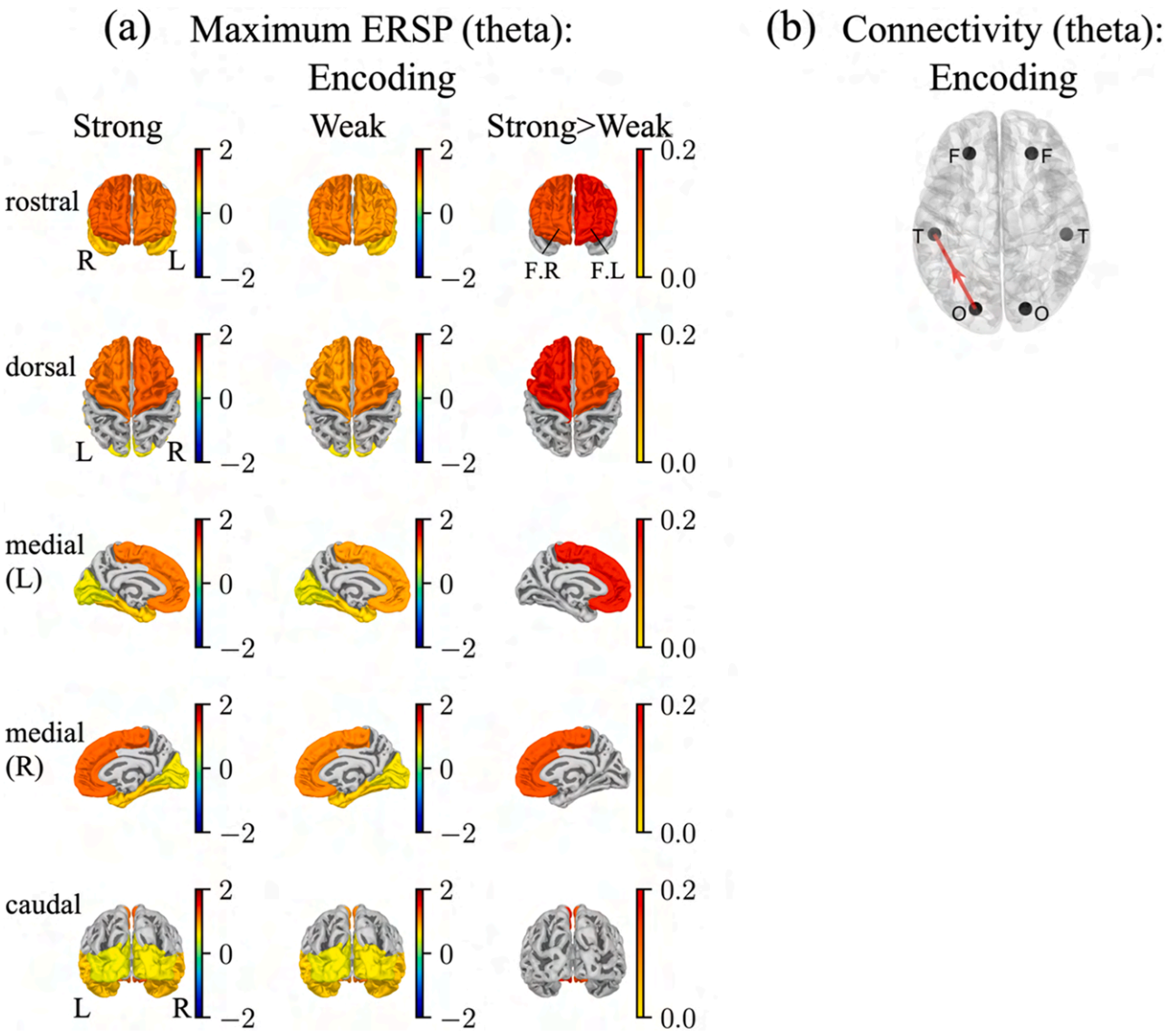

Fig. 4. Lobe-level results for theta-band during encoding: comparison of ERSP (panel a) and of connectivity (panel b) between strong and weak distractor conditions. *Panel a*: The first two columns show the grand-average ERSP in the theta band mapped onto the lobes (maximal perturbation inside the encoding TOI, lobe by lobe), separately for strong and weak distractor conditions. The gray portions in these two columns correspond to parietal lobes not included in this analysis. The third column shows the difference between the two distractor conditions, reporting the result of the performed statistical test: only the lobes that exhibited a significantly higher perturbation in strong vs. weak distractor condition ($p < 0.05$, uncorrected) are colored. Cortex views are reported by rows (rostral, dorsal, left-medial, right-medial, caudal, respectively). *Panel b*: Theta-band connectivity at lobe level. Each node represents a lobe (F: frontal, T: temporal, O: occipital) and the displayed directed edges indicate connections significantly higher for strong compared to weak distractors ($p < 0.05$, uncorrected).

columns in Fig. 5a). Interestingly, when tested statistically, alpha-ERSP resulted significantly higher in the right occipital lobe than in the left occipital lobe both in strong and in weak distractor condition (strong: $m_{R\text{-}L} = 0.23$, $SD_{R\text{-}L} = 0.52$, $p = 0.009$, $r = 0.56$; weak: $m_{R\text{-}L} = 0.29$, $SD_{R\text{-}L} = 0.47$, $p = 0.001$, $r = 0.68$; two-tail Wilcoxon signed-rank test). This right lateralization held also for the temporal lobes (strong: $m_{R\text{-}L} = 0.24$, $SD_{R\text{-}L} = 0.66$, $p = 0.0421$, $r = 0.44$; weak: $m_{R\text{-}L} = 0.32$, $SD_{R\text{-}L} = 0.62$, $p = 0.0239$, $r = 0.49$; two-tail Wilcoxon signed-rank test). No macro-ROI showed alpha-ERSP difference between the two distractor conditions, although it is noticeable a slight increase in the left occipital lobe in case of strong vs. weak distractor (last row in Fig. 5a). Conversely, a salient aspect here is that strong vs. weak distractors induced an increase in top-down connectivity coming from frontal and temporal lobes and targeting selectively the left occipital lobe (Fig. 5b, connectivity F.L→ O.L: $m_{S\text{-}W} = 0.0024$, $SD_{S\text{-}W} = 0.0049$, $p = 0.0156$, $r = 0.47$; connectivity T.R → O.L: $m_{S\text{-}W} = 0.0017$, $SD_{S\text{-}W} = 0.004$, $p = 0.0258$, $r = 0.42$; uncorrected p-values). This top-down connectivity modulation was accompanied by a significant increase in the in degree index of the left occipital lobe (Fig. 5c, $m_{S\text{-}W} = 0.0087$, $SD_{S\text{-}W} = 0.02$, $p = 0.0119$, $r = 0.49$, uncorrected p-value), which showed an increase in the entering connectivity from all other lobes in case if strong vs. weak distractors (although significant only from F.L and T.R). The out degree index of the macro-ROIs showed no difference in the alpha band during retention.

Connectivity results in the theta band during the retention TOI and in the alpha band during the encoding TOI, at the lobe level, are reported for completeness in Supplementary Materials (see Section S2, Fig. S6).

3.3. ROI-level analyses

ERSP results at the ROI level are shown in Fig. 6. As regarding the theta band in the encoding TOI (Fig. 6a), significant or close-to-significance higher theta-ERSP for strong vs. weak distractors was found especially in frontal ROIs, in agreement with lobe-level analysis in Fig. 4a (AC.R: $m_{S\text{-}W} = 0.18$, $SD_{S\text{-}W} = 0.41$, $p = 0.059$, $r = 0.34$; IF.L: $m_{S\text{-}W}$

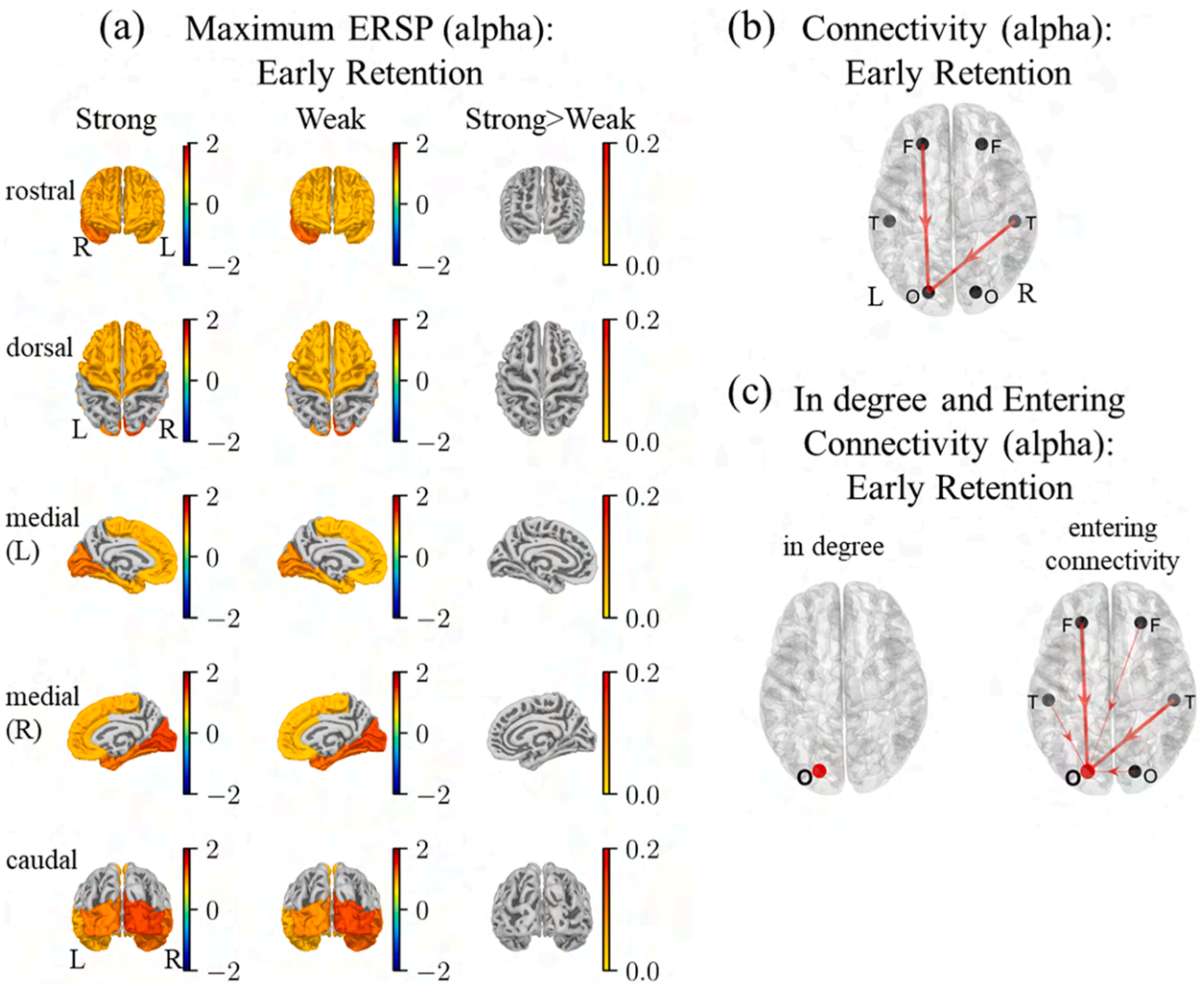

Fig. 5. Lobe-level results for alpha-band during early retention: comparison of ERSP (panel a) and of connectivity (panels b-d) between strong and weak distractor conditions. *Panel a*: The first two columns show the grand-average ERSP in the alpha band mapped onto the lobes (maximal perturbation inside the retention TOI, lobe by lobe), separately for strong and weak distractor conditions. The gray portions in these two columns correspond to parietal lobes not included in this analysis. The third column shows the difference between the two distractor conditions, reporting the result of the performed statistical test: only the lobes that exhibited a significantly higher perturbation in strong vs. weak distractor condition ($p < 0.05$, uncorrected) are colored (note that no lobe exhibited significance here). Cortex views are reported by rows (rostral, dorsal, left-medial, right-medial, caudal, respectively). *Panel b*: Each node represents a lobe (F: frontal, T: temporal, O: occipital) and the displayed directed edges indicate connections significantly higher for strong compared to weak distractors ($p < 0.05$, uncorrected). *Panel c*: Lobes with significantly higher ($p < 0.05$, uncorrected) in degree index in the strong vs. weak distractor condition (left panel) and connections entering into these lobes (right panel) higher for strong vs. weak distractors (thicker lines denote significant connections, $p < 0.05$, uncorrected).

$=0.24$, $SD_{S\text{-}W} = 0.54$, $p = 0.0036$, $r = 0.57$; PRC.L: $m_{S\text{-}W} = 0.14$, $SD_{S\text{-}W} = 0.44$, $p = 0.0516$, $r = 0.36$; PRC.R: $m_{S\text{-}W} = 0.11$, $SD_{S\text{-}W} = 0.28$, $p = 0.027$, $r = 0.42$; uncorrected p-values). This effect was observed also in posterior cingulate ROI and inferior temporal ROI (PC.L: $m_{S\text{-}W} = 0.16$, $SD_{S\text{-}W} = 0.47$, $p = 0.055$, $r = 0.35$; IT.L: $m_{S\text{-}W} = 0.15$, $SD_{S\text{-}W} = 0.39$, $p = 0.0516$, $r = 0.36$; uncorrected p-values). Among these ROIs, cingulate regions (AC.R, PC.L) and IF.L showed the highest difference in spectral perturbations for strong vs. weak distractors. As regarding alpha-ERSP, when considering strong and weak distractors separately (left and middle columns in Fig. 6b), the same right-hemisphere lateralization was seen as in lobe-level analysis, especially in temporal and occipital regions, (see also Fig. S6 in Section S2 of Supplementary Materials, further evidencing this right-hemisphere lateralization). When contrasting strong and weak distractor conditions, significant higher alpha-ERSP in case of strong vs. weak distractors was found in left temporal-occipital cortices (IT.L: $m_{S\text{-}W} = 0.14$, $SD_{S\text{-}W} = 0.2$, $p = 0.0036$, $r = 0.57$; LO.L: $m_{S\text{-}W} = 0.28$, $SD_{S\text{-}W} = 0.7$, $p = 0.04$, $r = 0.37$, uncorrected p-values), with the left lateral occipital ROI (LO.L) exhibiting the highest difference.

Figs. 7 and 8 show the results of the connectivity analysis at the ROI-level, respectively for the theta band in the encoding TOI and alpha band in the retention TOI. Specifically, each figure displays the ROIs that exhibited a significantly higher in degree or out degree in strong vs. weak distractors (panel a), and the connectivity patterns entering into (panel b) and exiting from (panel c) some of these ROIs.

In case of the theta band in the encoding TOI, the strong condition was characterized by a higher inflow (Fig. 7a, left map) in a few frontal and temporal ROIs, and by a higher outflow (Fig. 7a, right map) from a few frontal, temporal, and left occipital ROIs (in degree: corrected-$p \leq 0.0696$, uncorrected-$p \leq 0.0056$, $r \geq 0.56$; out degree: corrected-$p \leq 0.0455$, $r \geq 0.56$). The higher theta inflow/outflow at frontal ROIs was mainly due to increased connectivity from/to other frontal ROIs (see Fig. 7b and Fig. 7c-left map). In addition, the higher theta-outflow at temporal and occipital ROIs exhibited mainly a bottom-up pattern, from temporal (MTe.L, IT.R) to frontal ROIs (Fig. 7b-right map and Fig. 7c-right map), and from the left occipital (LO.L) to the right temporal cortex

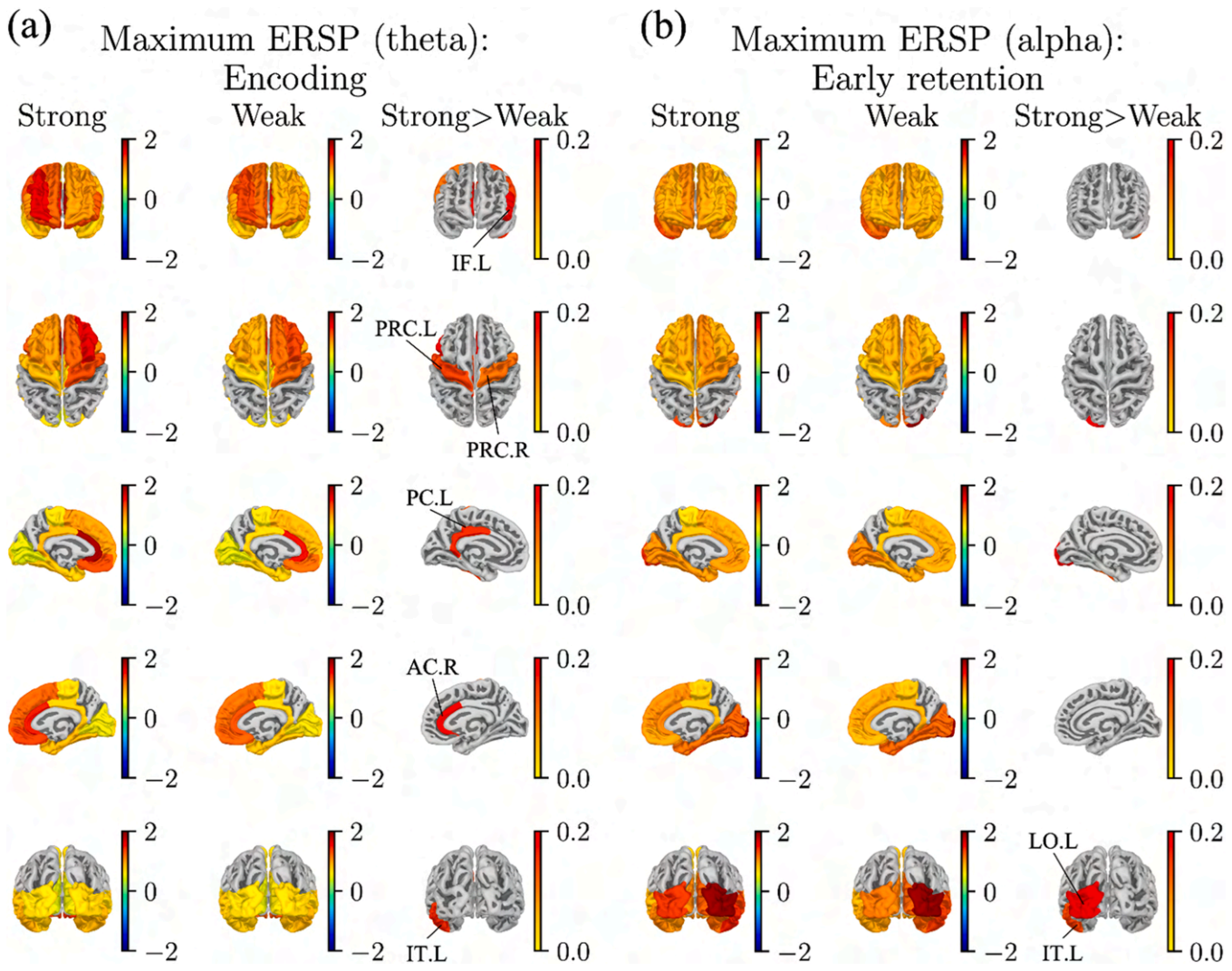

Fig. 6. ROI-level ERSP results: comparison of theta-band ERSP during encoding (panel a) and of alpha-band ERSP during early retention (panel b) between strong and weak distractor conditions. In each panel, the first two columns show the grand-average perturbations mapped onto the ROIs (maximal perturbation inside the TOI, ROI by ROI), separately for strong and weak distractor conditions. The gray portions in these two columns correspond to parietal lobes not included in this analysis. The third column shows the difference between the two distractor conditions, reporting the result of the performed statistical test: only the ROIs (in the frontal, temporal and occipital lobes) that exhibited a significantly higher perturbation in strong vs. weak distractor condition ($p < 0.05$, uncorrected) are colored. Cortex views are reported by rows as in Figs. 4a and 5a (rostral, dorsal, left-medial, right-medial, caudal, respectively).

(Fig. 7c-right map) (theta encoding sparse connectivity matrix: $p \leq 0.0476$, *Cohen's d* ≥ 0.37, *Cohen's d* $\leq$ -0.45). Finally, it is worth mentioning that some of the ROIs showing higher theta power in the encoding TOI for strong vs. weak distractors (e.g., AC.R, PC.L, PRC.R, IT.L, see Fig. 6a) were also involved in the connectivity pattern changes shown here.

As to the alpha band during retention, higher in degree and/or out degree for strong vs. weak distractors was obtained in a few frontal ROIs (AC.L, IF.L, OF.R), in temporal ROIs (STe.R, bilateral IT), and in a left occipital ROI (mO.L) (in degree: $p \leq 0.028$, $r \geq 0.6$; out degree: $p \leq 0.05$, $r \geq 0.6$; corrected p-values). The connectivity entering to/exiting from ROIs with significantly higher centrality indices exhibited some peculiar patterns (Fig. 8b and c). In particular, the strong distractor condition was associated with an increase in top-down connectivity, from frontal and temporal regions (AC.L, SFe.L, bilateral IF, OF.R, bilateral IT) towards left occipital regions (mO.L, LO.L, Fig. 8b right panel and Fig. 8c), confirming the results at lobe level (Fig. 5b). Furthermore, also frontal-to-temporal and temporal-to-frontal connectivity increased for strong vs. weak distractors (Fig.8b-left map and Fig.8c-left map), evidencing the involvement of recurrent (top-down and bottom-up) influences (alpha retention sparse connectivity matrix: $p \leq 0.0492$, *Cohen's d* ≥ 0.4, *Cohen's d* $\leq$ -0.32).

Connectivity results in the theta band during the retention TOI and in the alpha band during the encoding TOI, at the ROI-level, are reported for completeness in Supplementary Materials (see Section S2, Fig. S7).

4. Discussion

Protecting relevant information from distractors is crucial for successful working memory and more generally goal-oriented behavior. Deficits in protection-against-distraction seem to be key components of WM impairment in healthy aging and in neurological disorders, such as ADHD and schizophrenia (Lorenc et al., 2021). A better understanding of the neural mechanisms underlying distraction resistance in WM may not only enhance the comprehension of real-world human WM functions, but also contribute to an improved characterization of neurological disorders and cognitive decline, and to the definition of more effective interventions and training procedures. In this study, we analyzed the EEG source-level modulations of oscillatory power and connectivity, both in alpha-band and theta-band, in anticipation of

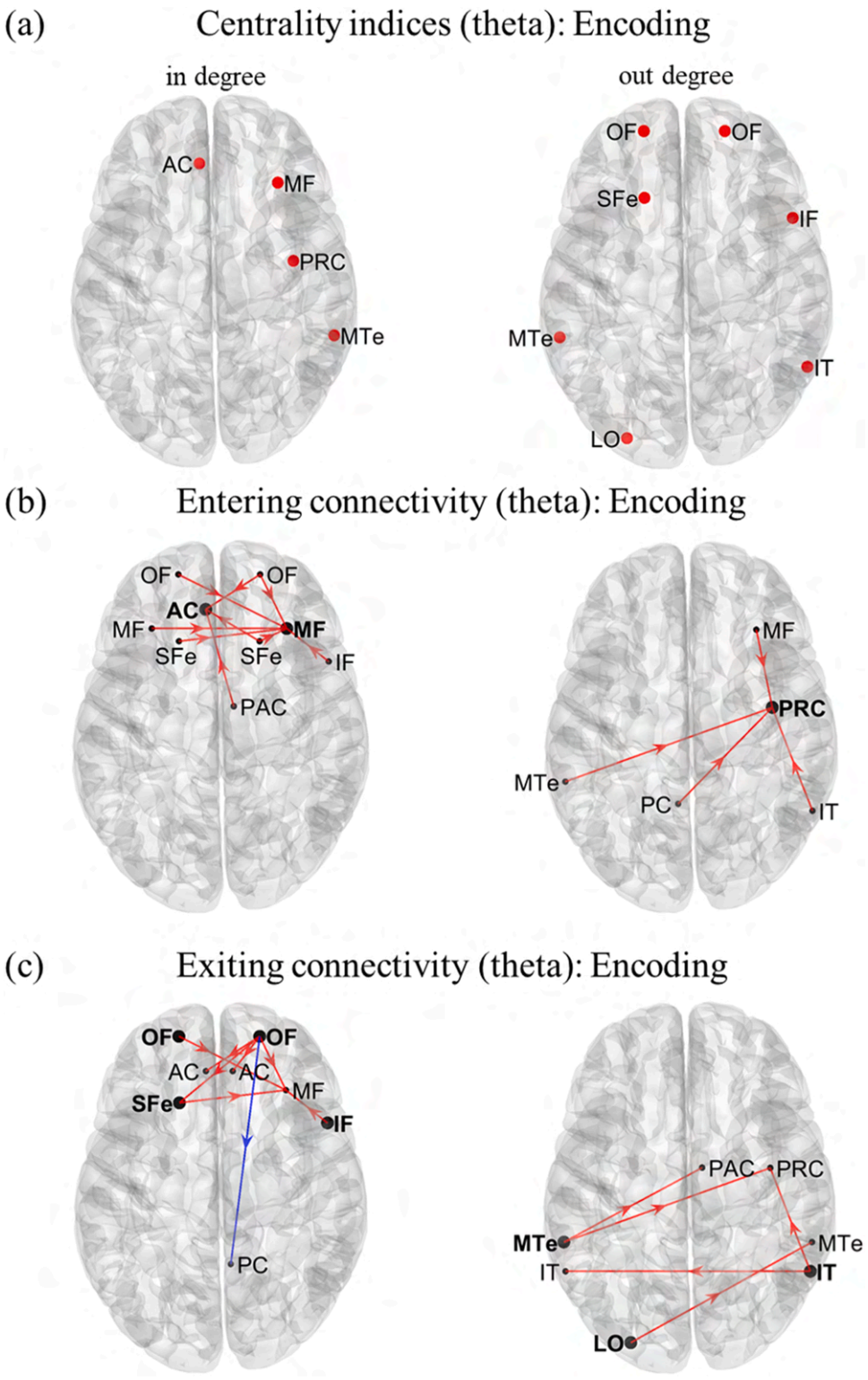

Fig. 7. ROI-level connectivity results: comparison of theta-band connectivity during encoding between strong and weak distractor conditions. *Panel a*: ROIs with close-to-significance higher in degree (left panel, corrected-p < 0.07) and significantly higher out degree (corrected-p < 0.05 right panel) in the strong vs. weak distractor condition, when considering theta-band connectivity in the encoding TOI. *Panel b*: Connections entering in a selection of ROIs with significant in degree (from panel a). Red/blue arrows denote an increased/decreased connectivity in the strong vs. weak distractor condition; only significant connections ($p < 0.05$) are displayed. *Panel c*: Connections departing from a selection of ROIs with significant out degree (from panel a). Red/blue arrows denote an increased/decreased connectivity in the strong vs. weak distractor condition; only significant connections ($p < 0.05$) are displayed.

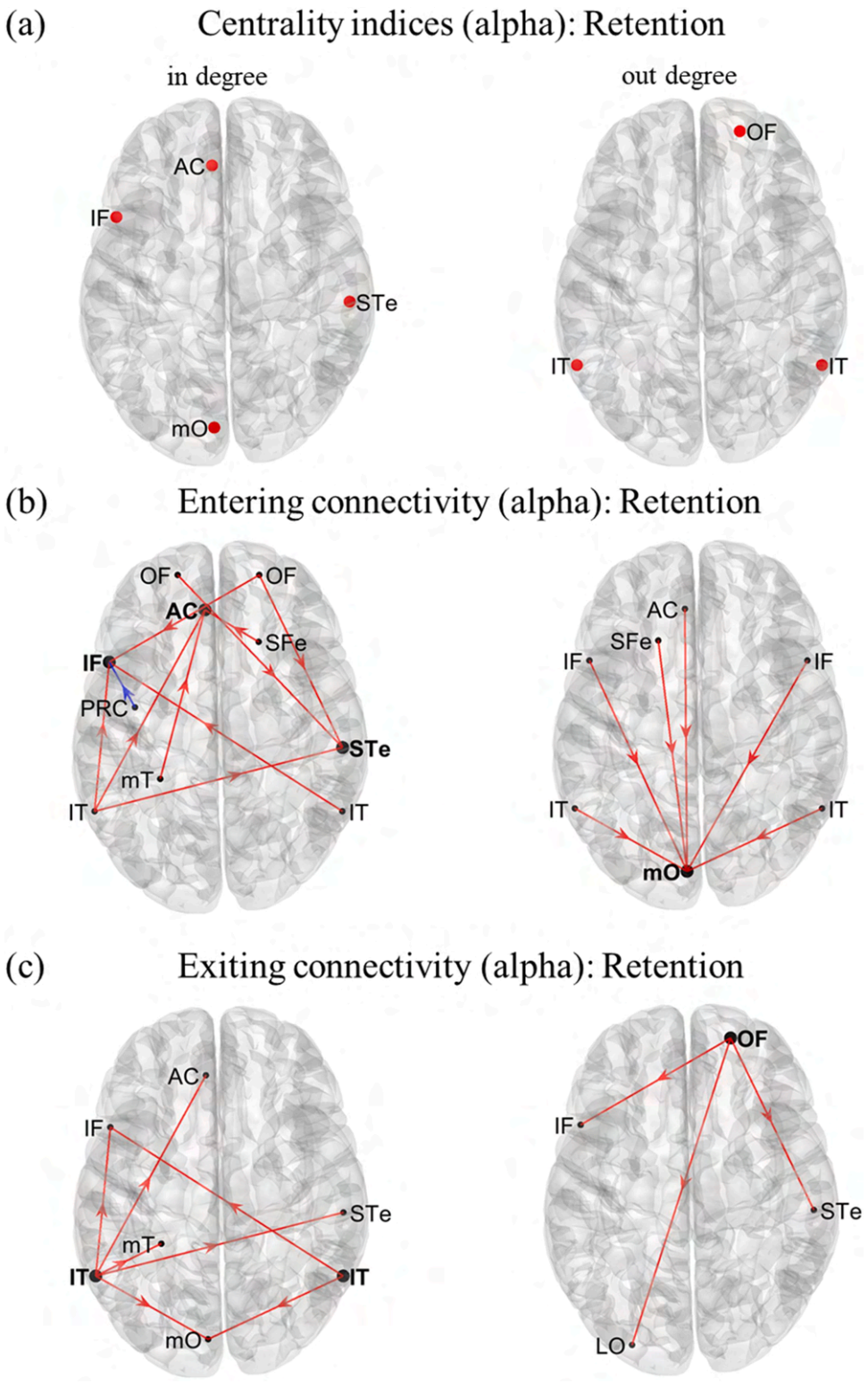

Fig. 8. ROI-level connectivity results: comparison of alpha-band connectivity during early retention between strong and weak distractor conditions. *Panel a*: ROIs with a significantly higher ($p < 0.05$, corrected) in degree (left panel) and out degree (right panel) in the strong vs. weak distractor condition, when considering alpha-band connectivity in the retention TOI. *Panel b*: Connections entering in a selection of ROIs with significant in degree (from panel a). Red/blue arrows denote an increased/decreased connectivity in the strong vs. weak distractor condition; only significant connections ($p < 0.05$) are displayed. *Panel c*: Connections departing from a selection of ROIs with significant out degree (from panel a). Red/blue arrows denote an increased/decreased connectivity in the strong vs. weak distractor condition; only significant connections ($p < 0.05$) are displayed.

distractors with different strength during a visual Sternberg-like working memory task involving verbal items (letters). Here, we focused on preparatory (proactive) oscillatory mechanisms that act in advance of distractor presentation when the nature and timing of the distractor can be anticipated, without examining oscillatory mechanisms in reaction to distractor appearance. The analyses were first performed at a coarser spatial resolution, considering macro-ROIs encompassing entire lobes, in order to reveal some main characteristics of the effects of distractor strength, and subsequently at a finer resolution (ROI-level).

4.1. Theta and alpha power modulation irrespective of distractor strength

First, general considerations can be derived from our results regardless of distractor strength (Figs. 4-6 and Figs. S1-S5 in Supplementary Materials). We obtained distributed increase in cortical theta power during encoding (Figs. 4a, 6a, S5a, but also retention, see Fig. S1 and S3), irrespective of distractors, with clearly larger effects at frontal regions, in particular prefrontal and anterior cingulate cortices. The latter are considered the regions principally involved in scalp midline frontal theta during working memory and other mental tasks (Cavanagh and Frank, 2014; Hsieh and Ranganath, 2014; Meltzer et al., 2008; Onton et al., 2005). Theta increase involving frontal but also other distributed regions, both during encoding and retention, is in line with previous studies (Jaiswal et al., 2010; Raghavachari et al., 2006, 2001; Sederberg et al., 2003). Differently from theta activity, increase in alpha power was limited to the retention phase, and assumed the highest values at occipital regions (Figs. 5a and 6b, see also Figs. S2, S4 and S5b), as commonly observed in visual WM tasks (Heinrichs-Graham and Wilson, 2015; Jensen et al., 2002; Khader et al., 2010; Wianda and Ross, 2019). Thus, overall, our data replicated common theta and alpha effects observed across previous WM studies. In addition, other interesting considerations can be drawn. In particular, the alpha power increase resulted biased towards the right hemisphere, in occipital and temporal regions, in both distractor conditions (Figs. 5a and 6b, see also Figs. S2, S4 and S5b). This result is reminiscent of alpha lateralization found in verbal (Butler and Glass, 1974; Galin et al., 1982) and spatial tasks (Loughnane et al., 2015), in particular in right-handed subjects, and associated with task-dependent hemisphere dominance. In particular, left occipital, temporal and also parietal lobes encompass areas that have been functionally associated with verbal processes. Processing and recognition of visually-presented verbal items (e.g., letters or digits) have been related to a lateralized activation in left lateral occipital and inferior temporal regions (Capilla et al., 2014; Flowers et al., 2004). Letter-selective responses have been observed in left inferior parietal cortex (Joseph et al., 2003). Moreover, the left transverse temporal gyrus and supramarginal gyrus are believed to be important nodes for phonological processing, also involved in grapheme-phoneme conversion, and to serve as core areas for subvocal rehearsal of verbal information (Deschamps et al., 2014; Fegen et al., 2015; Junker et al., 2023). Considering alpha as a marker of inhibition, the less alpha power observed during retention in these left regions can be interpreted by assuming that these areas, being dedicated to the extraction and encoding of features from the sensory input (visually presented letters), were engaged during the retention period too, in order to reactivate the representation of the no longer present input (de Vries et al., 2020). We hypothesize that during the retention phase, these left occipito-temporal areas were more subjected to antagonistic mechanisms than the right regions: on one hand, an inhibitory mechanism (operated by alpha increase) serving to disengage these areas to protect from impending intrusions, and on the other hand, an engagement mechanism (associated with alpha decrease) serving to maintain active processing in these areas for supporting memory trace maintenance. This interpretation remains mainly speculative here but, interestingly, is supported by some previous studies reporting specific alpha responses in left hemispheric regions during the storage of visually presented letters. For example, Heinrichs-Graham and Wilson (2015), during the maintenance of a set of displayed letters, obtained sustained alpha decrease in left middle and superior temporal gyri and supramarginal gyrus, throughout most of the maintenance phase. That study did not involve distractors presentation, thus the competition between the two antagonistic mechanisms may have been unbalanced towards alpha decrease. The study by Sghirripa et al. (2021), involving a task similar to ours with anticipated distractors, reported a significant increase in scalp alpha power immediately before distractor presentation above right occipito-temporal and parietal regions, whereas a minimal and non-significant increase was observed over the corresponding left regions. In that case, at variance with the previous mentioned study (Heinrichs-Graham and Wilson, 2015) and in line with our results (see Fig. 6b, first two columns), left alpha power did not show a decrease, possibly because of a stronger alpha inhibitory mechanism due to the anticipated distractors, contrasting alpha decrease. The antagonistic impact that different components of a task may have on alpha activity has also been emphasized in previous studies, although considering different types of tasks (Magosso et al., 2021, 2019).

4.2. Effect of distractor strength on theta-band power and connectivity

Theta power during encoding increased mainly in frontal and cingulate regions (Figs. 4a and 6a) for strong vs. weak distractors. The scaling of frontal theta increase with cognitive demand and control has been observed across several cognitive tasks (Cavanagh and Frank, 2014; Isabella et al., 2021; Womelsdorf et al., 2010). In WM tasks, frontal theta was found to increase with WM load in cingulate and prefrontal cortex (Onton et al., 2005; Proskovec et al., 2019); furthermore, higher frontal theta was reported in reaction to strong compared to weak distractors (i.e., during or after distractor presentation) both in a WM task (Fodor et al., 2020) and in target detection tasks (van Diepen et al., 2016). Here, we show that even the anticipation of distractors of different strength modulated theta activity, involving regions (such as the anterior cingulate cortex) known to be crucially involved in brain theta oscillations and associated with attentional and executive control processes (Cavanagh and Frank, 2014; Clayton et al., 2015).

Frontal regions during encoding were modulated by the distractor strength, not only in theta power but also in theta-band information inflow and outflow, with strong distractors being associated with stronger frontal-to-frontal connectivity (Fig. 7). Moreover, even if only marginally involved in power modulation, temporal and occipital regions exhibited increased exiting bottom-up connectivity (occipital to temporal and temporal to frontal) and also higher outdegree during encoding for strong vs. weak distractors (Figs. 4b and 7). The bottom-up connectivity patterns observed in our results resemble a flow of information from low-level sensory regions to higher-level regions for encoding progressively complex features of the input. An interesting aspect that emerges from our supplementary analyses is that the stronger involvement of frontal-to-frontal connectivity and bottom-up connectivity, for strong compared to weak distractors, appeared as a general feature of the theta band, characterizing not only the encoding phase but also the retention phase (Figs. S6 and S7 in Supplementary Materials). In the latter case, the increase in bottom-up connectivity occurred even to a greater extent (Fig. S7), and involved also increased occipital-to-frontal connectivity. Thus, overall, encoding and retention seemed to recruit similar theta-band mechanisms (local frontal mechanisms and bottom-up mechanisms) to proactively face strong impending distractors. A possible interpretation of these results is that the frontal theta mechanisms were related to more general processes of attention allocation (not strictly involving memory processes), while the bottom-up connectivity from occipital and temporal regions was more related to encoding and memory processes. In particular, the increase in local frontal power and frontal-to-frontal connectivity might mark more sustained attention allocation both during encoding and retention, associated with the anticipation of the strong distractor. During encoding, the increased bottom-up theta connectivity might reflect a stronger bottom-up relay of

sensory information along the hierarchical ventral visual pathway up to the prefrontal cortex, to enhance the ongoing representation of the stimulus to be kept in memory. During retention, the increased bottom-up theta connectivity might contribute to implement a stronger reactivation of the same representations of the removed stimulus. This interpretation, though tentative, has some counterparts in the literature. Recent studies support a predominant bottom-up directionality of the visual theta in the primate brain, from lower to higher levels of the visual cortex and to the temporal cortex (Spyropoulos et al., 2018), and TMS studies indicated the involvement of a bottom-up network from sensory to frontal regions in WM (Miyauchi et al., 2016). Moreover, results of a task designed to differently modulate task complexity and memory load, suggested frontal midline theta activity to be related to general sustained attentional mechanisms and to be functionally dissociated from long-range theta interactions (Sauseng et al., 2007). Other WM studies hypothesized a functional separation between frontal theta activity, as a correlate of general attentional processing, and a more posterior theta-organized network for memory formation and maintenance (Khader et al., 2010; Raghavachari et al., 2006).

4.3. Effect of distractor strength on alpha-band power and connectivity

Alpha power during retention increased for strong relative to weak distractors in only a few occipital-temporal regions (Fig. 6b), precluding to obtain any power effect at lobe level (Fig. 5a) Although we acknowledge that our results may be affected by some amount of spatial inaccuracy, it appears remarkable that the alpha-modulated ROIs included the left lateral occipital cortex and the left inferior temporal gyrus (see Fig. 6b), which are known to be engaged in letter processing (and thus also in processing the strong distractors, too). Thus, our results appear consistent with the hypothesis that alpha power has a role in suppressing distracting information, via anticipatory inhibition of specific representational areas. Our results match the findings obtained in a MEG study by Bonnefond and Jensen (2012), who used a task similar to ours, except for the modality of the memory set presentation (letters presented sequentially rather than simultaneously): the authors found a significant anticipatory alpha power increase for strong vs. weak distractors in left parietal-occipital sensors, and localized the source in left occipital-temporal cortices. In contrast to Bonnefond and Jensen (2012), the more recent EEG study by Sghirripa et al. (2021), using a task like ours (i.e., with the letters of the memory set presented simultaneously) and performing only a sensor-level analysis, failed to find an alpha power modulation by distractor strength and attributed this inconsistent result to differences in task features related to the different way of memory set presentation (simultaneously vs. sequentially). Here, we did not find any effect at the scalp-level (as in Sghirripa et al., 2021), while at the cortex-level our results resembled those obtained by Bonnefond and Jensen (2012). Thus, based on our results, it may be possible that differences in task features might lead to stronger alpha effects in one case (sequential item presentation), detectable also at the sensor-level, than in the other case (simultaneous item presentation), where the effects could remain masked at the scalp-level but emerge at the source-level. Thus, source-level analysis may be able to capture effects that are not or hardly detectable at the scalp-level, helping to reconcile contrasting or dissimilar results.

The performed connectivity analyses suggested the involvement of top-down alpha influences targeting left posterior sensory areas during retention. Indeed, in contrast to the theta band, which is predominantly characterized by a modulation of bottom-up connectivity, the alpha band during retention exhibited a distinctive increase in top-down frontal-to-occipital and temporal-to-occipital connectivity (Figs. 5b, 5c, 8) for strong vs. weak distractors, primarily targeting left occipital regions. Top-down influences from frontal to posterior sensory areas were reported previously across several tasks (working memory, visuospatial, mental arithmetic tasks) (e.g. see Doesburg et al., 2016; Magosso et al., 2021; Wang et al., 2016), and related to the inhibition of sensory processing to gate out interfering sensory inputs. Here, we confirm these findings and extend them by reporting for the first time a modulation of top-down alpha-band connectivity according to distractor strength. Top-down alpha connectivity increase during retention was also accompanied by an increase in bidirectional (bottom-up and top-down) frontal-temporal connections (Figs. 8b and c). Bidirectional top-down and bottom-up alpha influences were reported previously as characteristic of an internal attention task relative to external attention (Magosso et al., 2021), and could contribute to reduce visual interference. Thus, overall, during retention, increased theta-band bottom-up influences would operate to enhance the internal memorized representation in anticipation of strong distractors, and increased top-down (but also bottom-up) alpha-band influences would operate to protect this internal representation by inhibiting the processing of impending distractors. Remarkably, this recurrent pattern of increased connectivity both top-down and bottom-up, for strong vs. weak distractors, was specific to the alpha-band and the retention phase only and did not occur during encoding (no ROI exhibited an increase in in degree or out degree indices for strong vs. weak distractors in alpha band during encoding; see Supplementary Materials). In this way, during encoding, bottom-up theta-band influences operate to strengthen the representation of the ongoing task-relevant stimulus, without alpha-mediated inhibitory influences over sensory regions, which could decrease the processing of the ongoing target stimulus.

4.4. Limitations and future directions

This study presents some limitations that can be overcome in future investigations.

First, we acknowledge that EEG source localization improves with high electrode density and when using individualized head models (Michel and Brunet, 2019), while here we adopted a template head model and we used 60 electrodes, with data rank further reduced by the procedure for artifact removal. For this reason, we avoided the analysis at small cortical parcels, and we focused on modulation of power and of connectivity patterns at the level of larger cortical patches, founding some promising matching between our results and existing literature. Indeed, as discussed above, results of power and connectivity analyses across distractor conditions pointed to areas (mainly frontal areas and cingulate cortex for theta-band, left temporal-occipital cortex for alpha-band) in line with the current knowledge about the phenomena under investigations and matching existing findings. Undoubtedly, future investigations utilizing a greater number of electrodes and subject-specific head models may be useful for performing analyses at a finer spatial scale and for improving the present findings.

Another possible limit is that we might have underestimated the effect of strong vs. weak distractors, since all trials in every block was included in the analyses, without disregarding the first trial of each block.

Another aspect concerns the lack of investigation of other rhythms. Indeed, there are findings that suggest a role of beta rhythm (13–30 Hz) in WM processes (Hwang et al., 2005; Koshy et al., 2020; Proskovec et al., 2019; Schmidt et al., 2019), and our data too exhibited the involvement of part of the beta-band (in particular of the low beta-band) during retention (see Figs. S1-S4 in Supplementary Materials). Moreover, gamma rhythm (30–100 Hz) and theta-gamma coupling are known to be key mechanisms supporting the simultaneous representation of multiple items (Lisman and Jensen, 2013), and enhanced gamma oscillations have been widely related to WM functions (see Roux and Uhlhaas, 2014 for a review). Thus, future studies could examine the effects of distractor strength on beta and gamma oscillations, thereby enhancing the functional interpretation of these two rhythms and the mechanistic comprehension of protection from distractors.

Finally, behavioral data were used to check whether the participants were actually engaged into the task, as confirmed by the high response accuracy, and by values of both accuracy and reaction time comparable

with those reported in previous studies (Bonnefond and Jensen, 2012; Sghirripa et al., 2021). We also tested for the existence of a correlation between electrophysiological measures (power or connectivity in theta band or alpha band) and behavioral performance (reaction time and accuracy) across subjects. Unfortunately, the tests performed did not provide significant results. This is at variance with the study by Bonnefond and Jensen (2012) who found a negative correlation between the reaction time and the occipital alpha power immediately preceding the distractor presentation. It is possible that differences between our experimental protocol and that of Bonnefond and Jensen (2012) contributed to this discrepancy. Indeed, in that study, the items of the memory set were presented sequentially and not simultaneously (as here); moreover, the interval separating the probe and the pre-distractor retention (where alpha power was evaluated) was only 1.13 s, while in our study the probe was separated from the pre-distractor retention by 3 seconds. The sequential presentation of the items to be remembered could be a more demanding condition than simultaneous presentation, and may have facilitated the emergence of a behavioral effect. Moreover, we claim that due to the relative long interval from the phases we examined and the behavioral performances ($>$ 3 s), a trustworthy analysis of the relationship between behavior and oscillatory measures in our task would require considering the other phases not included in the present investigation, i.e., the distractor presentation phase and the late retention phase. Indeed, while in this study we limited the investigation to the oscillatory mechanisms in the phases preceding the distractors, also the oscillatory states in reaction to the distractors (during and after distractor presentation) likely affect behavioral performances in a relevant manner.

5. Conclusions

In conclusion, the present study investigates the modulatory effect of the strength of anticipated distractors on theta and alpha oscillatory mechanisms during a WM task, focusing on the increase in power and connectivity induced by strong vs. weak distractors. Novelty points concern the joint investigation of both rhythms and connectivity analysis. Indeed, previous studies have investigated oscillatory alpha power in relation to anticipated distractor strength (albeit with some discrepancies in results), but they neglected theta power investigation and did not explore the impact of distractor strength on connectivity patterns in any band. We found that the strength of anticipated distractors modulated power and connectivity in both bands, with connectivity modulation exhibiting distinctive patterns in the encoding and retention phases. During encoding, theta power in frontal regions was enhanced by strong distractors and associated with increased frontal-to-frontal and bottom-up occipital-to-temporal-to-frontal connectivity. This modulation of theta connectivity was even strengthened during retention. These theta mechanisms could mediate increased attentional control and enhancement of target stimulus representation, both during encoding and retention. During retention, but not during encoding, alpha power increased in occipital-temporal regions for strong vs. weak distractors and was associated with increased top-down frontal-to-occipital and temporal-to-occipital connectivity. These alpha mechanisms during retention likely mediate increased inhibition of sensory areas to suppress the processing of an imminent strong distractor, protecting the stored target representation, but without operating increased inhibitory influences during encoding, to prevent deterioration of the ongoing target representation.

Overall, we postulate that the preparation for distractors involves two components: an enhancement of target representation and an inhibition of the processing of imminent distracting information. In this view, theta-band and alpha-band mechanisms cooperate proactively to actualize these components via a dynamical organization of functional communication patterns, simultaneously operating at different frequency bands. This study may contribute to enhance our comprehension of the functional significance of theta and alpha rhythm, and to a better understanding of the relationships between oscillatory activity and WM functions and dysfunctions, an issue that could have relevant implications for the treatment of WM impairment in neurological patients.

CRediT authorship contribution statement

Elisa Magosso: Conceptualization, Writing – review & editing, Writing – original draft, Validation, Supervision, Resources, Project administration, Methodology, Formal analysis, Software, Visualization. **Davide Borra:** Conceptualization, Writing – review & editing, Writing – original draft, Visualization, Software, Methodology, Investigation, Formal analysis, Data curation.

Declaration of competing interest

The authors declare that they have no known competing financial interests or personal relationships that could have appeared to influence the work reported in this paper.

Data availability

Data will be made available on request.

Acknowledgments

This work was supported by #NEXTGENERATIONEU (NGEU) and funded by the Ministry of University and Research (MUR), National Recovery and Resilience Plan (NRRP), project MNESYS (PE0000006) — A Multiscale integrated approach to the study of the nervous system in health and disease (DN. 1553 11.10.2022).

The authors gratefully acknowledge Maria Santoro, Serena Angelica Mori, and Annalisa Taddei for their help in EEG recordings.

Supplementary materials

Supplementary material associated with this article can be found, in the online version, at doi:10.1016/j.neuroimage.2024.120835.

References

Anticevic, A., Repovs, G., Krystal, J.H., Barch, D.M., 2012. A broken filter: prefrontal functional connectivity abnormalities in schizophrenia during working memory interference. Schizophr. Res. 141, 8–14. https://doi.org/10.1016/j.schres.2012.07.007.

Aurtenetxe, S., García-Pacios, J., del Río, D., López, M.E., Pineda-Pardo, J.A., Marcos, A., Delgado Losada, M.L., López-Frutos, J.M., Maestú, F., 2016. Interference impacts working memory in mild cognitive impairment. Front. Neurosci. 10, 443. https://doi.org/10.3389/fnins.2016.00443.

Benjamini, Y., Yekutieli, D., 2001. The control of the false discovery rate in multiple testing under dependency. Annals Statistics 29, 1165–1188.

Bonnefond, M., Jensen, O., 2012. Alpha oscillations serve to protect working memory maintenance against anticipated distracters. Curr. Biol. 22, 1969–1974. https://doi.org/10.1016/j.cub.2012.08.029.

Borra, D., Fantozzi, S., Bisi, M.C., Magosso, E., 2023. Modulations of cortical power and connectivity in alpha and beta bands during the preparation of reaching movements. Sensors. (Basel) 23, 3530. https://doi.org/10.3390/s23073530.

Brkić, D., Sommariva, S., Schuler, A.-L., Pascarella, A., Belardinelli, P., Isabella, S.L., Pino, G.D., Zago, S., Ferrazzi, G., Rasero, J., Arcara, G., Marinazzo, D., Pellegrino, G., 2023. The impact of ROI extraction method for MEG connectivity estimation: practical recommendations for the study of resting state data. Neuroimage 284, 120424. https://doi.org/10.1016/j.neuroimage.2023.120424.

Butler, S.R., Glass, A., 1974. Asymmetries in the electroencephalogram associated with cerebral dominance. Electroencephalogr. Clin. Neurophysiol. 36, 481–491. https://doi.org/10.1016/0013-4694(74)90205-3.

Capilla, A., Schoffelen, J.-M., Paterson, G., Thut, G., Gross, J., 2014. Dissociated α-band modulations in the dorsal and ventral visual pathways in visuospatial attention and perception. Cereb. Cortex 24, 550–561. https://doi.org/10.1093/cercor/bhs343.

Cavanagh, J.F., Frank, M.J., 2014. Frontal theta as a mechanism for cognitive control. Trends. Cogn. Sci. 18, 414–421. https://doi.org/10.1016/j.tics.2014.04.012.

Clayton, M.S., Yeung, N., Cohen Kadosh, R., 2015. The roles of cortical oscillations in sustained attention. Trends. Cogn. Sci. 19, 188–195.

Dai, Z., de Souza, J., Lim, J., Ho, P.M., Chen, Y., Li, J., Thakor, N., Bezerianos, A., Sun, Y., 2017. EEG cortical connectivity analysis of working memory reveals topological reorganization in theta and alpha bands. Front. Hum. Neurosci. 11, 237. https://doi.org/10.3389/fnhum.2017.00237.

de Vries, I.E.J., Savran, E., van Driel, J., Olivers, C.N.L., 2019. Oscillatory mechanisms of preparing for visual distraction. J. Cogn. Neurosci. 31, 1873–1894. https://doi.org/10.1162/jocn_a_01460.

de Vries, I.E.J., Slagter, H.A., Olivers, C.N.L., 2020. Oscillatory control over representational states in working memory. Trends. Cogn. Sci. 24, 150–162. https://doi.org/10.1016/j.tics.2019.11.006.

Deschamps, I., Baum, S.R., Gracco, V.L., 2014. On the role of the supramarginal gyrus in phonological processing and verbal working memory: evidence from rTMS studies. Neuropsychologia 53, 39–46. https://doi.org/10.1016/j.neuropsychologia.2013.10.015.

Desikan, R.S., Ségonne, F., Fischl, B., Quinn, B.T., Dickerson, B.C., Blacker, D., Buckner, R.L., Dale, A.M., Maguire, R.P., Hyman, B.T., Albert, M.S., Killiany, R.J., 2006. An automated labeling system for subdividing the human cerebral cortex on MRI scans into gyral based regions of interest. Neuroimage 31, 968–980. https://doi.org/10.1016/j.neuroimage.2006.01.021.

Doesburg, S.M., Bedo, N., Ward, L.M., 2016. Top-down alpha oscillatory network interactions during visuospatial attention orienting. Neuroimage 132, 512–519. https://doi.org/10.1016/j.neuroimage.2016.02.076.

Fegen, D., Buchsbaum, B.R., D'Esposito, M., 2015. The effect of rehearsal rate and memory load on verbal working memory. Neuroimage 105, 120. https://doi.org/10.1016/j.neuroimage.2014.10.034.

Fischler, M.A., Bolles, R.C., 1981. Random sample consensus: a paradigm for model fitting with applications to image analysis and automated cartography. Commun. ACM 24, 381–395. https://doi.org/10.1145/358669.358692.

Flowers, D.L., Jones, K., Noble, K., VanMeter, J., Zeffiro, T.A., Wood, F.B., Eden, G.F., 2004. Attention to single letters activates left extrastriate cortex. Neuroimage 21, 829–839. https://doi.org/10.1016/j.neuroimage.2003.10.002.

Fodor, Z., Marosi, C., Tombor, L., Csukly, G., 2020. Salient distractors open the door of perception: alpha desynchronization marks sensory gating in a working memory task. Sci. Rep. 10, 19179. https://doi.org/10.1038/s41598-020-76190-3.

Foxe, J.J., Snyder, A.C., 2011. The role of alpha-band brain oscillations as a sensory suppression mechanism during selective attention. Front. Psychol. 2, 154. https://doi.org/10.3389/fpsyg.2011.00154.

Frey, J.N., Ruhnau, P., Weisz, N., 2015. Not so different after all: The same oscillatory processes support different types of attention. Brain Res. 1626, 183–197.

Fu, K.M., Foxe, J.J., Murray, M.M., Higgins, B.A., Javitt, D.C., Schroeder, C.E., 2001. Attention-dependent suppression of distracter visual input can be cross-modally cued as indexed by anticipatory parieto-occipital alpha-band oscillations. Brain Res. Cogn. Brain Res. 12, 145–152. https://doi.org/10.1016/s0926-6410(01)00034-9.

Galin, D., Ornstein, R., Herron, J., Johnstone, J., 1982. Sex and handedness differences in EEG measures of hemispheric specialization. Brain Lang. 16, 19–55. https://doi.org/10.1016/0093-934X(82)90070-0.

Geweke, J., 1982. Measurement of linear dependence and feedback between multiple time series. J. Am. Stat. Assoc. 77, 304–313. https://doi.org/10.1080/01621459.1982.10477803.

Ghumare, E.G., Schrooten, M., Vandenberghe, R., Dupont, P., 2018. A time-varying connectivity analysis from distributed EEG sources: a simulation study. Brain Topogr. 31, 721–737. https://doi.org/10.1007/s10548-018-0621-3.

Gramfort, A., Luessi, M., Larson, E., Engemann, D.A., Strohmeier, D., Brodbeck, C., Goj, R., Jas, M., Brooks, T., Parkkonen, L., Hämäläinen, M., 2013. MEG and EEG data analysis with MNE-Python. Front. Neurosci. 7, 267. https://doi.org/10.3389/fnins.2013.00267.

Grandchamp, R., Delorme, A., 2011. Single-trial normalization for event-related spectral decomposition reduces sensitivity to noisy trials. Front. Psychol. 2, 236. https://doi.org/10.3389/fpsyg.2011.00236.

Granger, C.W.J., 1969. Investigating causal relations by econometric models and cross-spectral. Methods. Econometrica 37, 424. https://doi.org/10.2307/1912791.

Heinrichs-Graham, E., Wilson, T.W., 2015. Spatiotemporal oscillatory dynamics during the encoding and maintenance phases of a visual working memory task. Cortex 69, 121–130. https://doi.org/10.1016/j.cortex.2015.04.022.

Hsieh, L.-T., Ranganath, C., 2014. Frontal midline theta oscillations during working memory maintenance and episodic encoding and retrieval. Neuroimage 85 (Pt 2), 721–729. https://doi.org/10.1016/j.neuroimage.2013.08.003.

Hwang, G., Jacobs, J., Geller, A., Danker, J., Sekuler, R., Kahana, M.J., 2005. EEG correlates of verbal and nonverbal working memory. Behav. Brain Functions 1, 20. https://doi.org/10.1186/1744-9081-1-20.

Isabella, S.L., Cheyne, J.A., Cheyne, D., 2021. Inhibitory control in the absence of awareness: interactions between frontal and motor cortex oscillations mediate implicitly learned responses. Front. Hum. Neurosci. 15, 786035 https://doi.org/10.3389/fnhum.2021.786035.

Jaiswal, N., Ray, W., Slobounov, S., 2010. Encoding of visual-spatial information in working memory requires more cerebral efforts than retrieval: evidence from eeg and virtual reality study. Brain Res. 1347, 80–89. https://doi.org/10.1016/j.brainres.2010.05.086.

Jensen, O., Gelfand, J., Kounios, J., Lisman, J.E., 2002. Oscillations in the alpha band (9-12 Hz) increase with memory load during retention in a short-term memory task. Cereb. Cortex. 12, 877–882. https://doi.org/10.1093/cercor/12.8.877.

Jensen, O., Mazaheri, A., 2010. Shaping functional architecture by oscillatory alpha activity: gating by inhibition. Front. Hum. Neurosci. 4, 186. https://doi.org/10.3389/fnhum.2010.00186.

Jensen, O., Tesche, C.D., 2002. Frontal theta activity in humans increases with memory load in a working memory task. Eur. J. Neurosci. 15, 1395–1399. https://doi.org/10.1046/j.1460-9568.2002.01975.x.

Jokisch, D., Jensen, O., 2007. Modulation of gamma and alpha activity during a working memory task engaging the dorsal or ventral stream. J. Neurosci. 27, 3244–3251. https://doi.org/10.1523/JNEUROSCI.5399-06.2007.

Joseph, J.E., Gathers, A.D., Piper, G.A., 2003. Shared and dissociated cortical regions for object and letter processing. Brain Res. Cogn. Brain Res. 17, 56–67. https://doi.org/10.1016/s0926-6410(03)00080-6.

Junker, F.B., Schlaffke, L., Lange, J., Schmidt-Wilcke, T., 2023. The angular gyrus serves as an interface between the non-lexical reading network and the semantic system: evidence from dynamic causal modeling. Brain Struct. Funct. https://doi.org/10.1007/s00429-023-02624-z.

Khader, P.H., Jost, K., Ranganath, C., Rösler, F., 2010. Theta and Alpha oscillations during working-memory maintenance predict successful long-term memory encoding. Neurosci. Lett. 468, 339–343. https://doi.org/10.1016/j.neulet.2009.11.028.

Klimesch, W., 1999. EEG alpha and theta oscillations reflect cognitive and memory performance: a review and analysis. Brain Res. Brain Res. Rev. 29, 169–195. https://doi.org/10.1016/s0165-0173(98)00056-3.

Klimesch, W., Doppelmayr, M., Schwaiger, J., Auinger, P., Winkler, T., 1999. Paradoxical" alpha synchronization in a memory task. Brain Res. Cogn. Brain Res. 7, 493–501. https://doi.org/10.1016/s0926-6410(98)00056-1.

Koshy, S.M., Wiesman, A.I., Proskovec, A.L., Embury, C.M., Schantell, M.D., Eastman, J. A., Heinrichs-Graham, E., Wilson, T.W., 2020. Numerical working memory alters alpha-beta oscillations and connectivity in the parietal cortices. Hum. Brain Mapp. 41, 3709–3719. https://doi.org/10.1002/hbm.25043.

Kustermann, T., Rockstroh, B., Miller, G.A., Popov, T., 2018. Neural network communication facilitates verbal working memory. Biol. Psychol. 136, 119–126. https://doi.org/10.1016/j.biopsycho.2018.05.018.

Lee, T.W., Girolami, M., Sejnowski, T.J., 1999. Independent component analysis using an extended infomax algorithm for mixed subgaussian and supergaussian sources. Neural Comput. 11, 417–441. https://doi.org/10.1162/089976699300016719.

Lisman, J.E., Jensen, O., 2013. The theta-gamma neural code. Neuron 77, 1002–1016. https://doi.org/10.1016/j.neuron.2013.03.007.

Lorenc, E.S., Mallett, R., Lewis-Peacock, J.A., 2021. Distraction in visual working memory: resistance is not futile. Trends. Cogn. Sci. 25, 228–239. https://doi.org/10.1016/j.tics.2020.12.004.

Loughnane, G.M., Shanley, J.P., Lalor, E.C., O'Connell, R.G., 2015. Behavioral and electrophysiological evidence of opposing lateral visuospatial asymmetries in the upper and lower visual fields. Cortex 63, 220–231. https://doi.org/10.1016/j.cortex.2014.09.003.

Magosso, E., De Crescenzio, F., Ricci, G., Piastra, S., Ursino, M., 2019. EEG Alpha Power Is Modulated by Attentional Changes during Cognitive Tasks and Virtual Reality Immersion. Comput. Intell. Neurosci., 7051079 https://doi.org/10.1155/2019/7051079, 2019.

Magosso, E., Ricci, G., Ursino, M., 2021. Alpha and theta mechanisms operating in internal-external attention competition. J. Integr. Neurosci. 20, 1–19. https://doi.org/10.31083/j.jin.2021.01.422.

McNab, F., Zeidman, P., Rutledge, R.B., Smittenaar, P., Brown, H.R., Adams, R.A., Dolan, R.J., 2015. Age-related changes in working memory and the ability to ignore distraction. Proc. Natl. Acad. Sci. u S. a 112, 6515–6518. https://doi.org/10.1073/pnas.1504162112.

Meltzer, J.A., Zaveri, H.P., Goncharova, I.I., Distasio, M.M., Papademetris, X., Spencer, S. S., Spencer, D.D., Constable, R.T., 2008. Effects of working memory load on oscillatory power in human intracranial EEG. Cereb. Cortex. 18, 1843–1855. https://doi.org/10.1093/cercor/bhm213.

Michel, C.M., Brunet, D., 2019. EEG source imaging: a practical review of the analysis steps. Front. Neurol. 10, 325. https://doi.org/10.3389/fneur.2019.00325.

Miyauchi, E., Kitajo, K., Kawasaki, M., 2016. TMS-induced theta phase synchrony reveals a bottom-up network in working memory. Neurosci. Lett. 622, 10–14. https://doi.org/10.1016/j.neulet.2016.04.008.

Nichols, T.E., Holmes, A.P., 2002. Nonparametric permutation tests for functional neuroimaging: a primer with examples. Hum. Brain Mapp. 15, 1–25. https://doi.org/10.1002/hbm.1058.

Noonan, M.P., Crittenden, B.M., Jensen, O., Stokes, M.G., 2018. Selective inhibition of distracting input. Behav. Brain Res. 355, 36–47. https://doi.org/10.1016/j.bbr.2017.10.010. SI: MCC 2016.

Onton, J., Delorme, A., Makeig, S., 2005. Frontal midline EEG dynamics during working memory. Neuroimage 27, 341–356. https://doi.org/10.1016/j.neuroimage.2005.04.014.

Pascual-Marqui, R.D., Lehmann, D., Koukkou, M., Kochi, K., Anderer, P., Saletu, B., Tanaka, H., Hirata, K., John, E.R., Prichep, L., Biscay-Lirio, R., Kinoshita, T., 2011. Assessing interactions in the brain with exact low-resolution electromagnetic tomography. Philos. Trans. a Math. Phys. Eng. Sci. 369, 3768–3784. https://doi.org/10.1098/rsta.2011.0081.

Pavlov, Y.G., Kotchoubey, B., 2022. Oscillatory brain activity and maintenance of verbal and visual working memory: a systematic review. Psychophysiology. 59, e13735. https://doi.org/10.1111/psyp.13735.

Payne, L., Guillory, S., Sekuler, R., 2013. Attention-modulated alpha-band oscillations protect against intrusion of irrelevant information. J. Cogn. Neurosci. 25, 1463–1476. https://doi.org/10.1162/jocn_a_00395.

Postle, B.R., 2006. Working memory as an emergent property of the mind and brain. Neuroscience 139, 23–38. https://doi.org/10.1016/j.neuroscience.2005.06.005.

Proskovec, A.L., Heinrichs-Graham, E., Wilson, T.W., 2019. Load modulates the alpha and beta oscillatory dynamics serving verbal working memory. Neuroimage 184, 256–265. https://doi.org/10.1016/j.neuroimage.2018.09.022.

Raghavachari, S., Kahana, M.J., Rizzuto, D.S., Caplan, J.B., Kirschen, M.P., Bourgeois, B., Madsen, J.R., Lisman, J.E., 2001. Gating of human theta oscillations by a working memory task. J. Neurosci. 21, 3175–3183. https://doi.org/10.1523/JNEUROSCI.21-09-03175.2001.

Raghavachari, S., Lisman, J.E., Tully, M., Madsen, J.R., Bromfield, E.B., Kahana, M.J., 2006. Theta oscillations in human cortex during a working-memory task: evidence for local generators. J. Neurophysiol. 95, 1630–1638. https://doi.org/10.1152/jn.00409.2005.

Riddle, J., Scimeca, J.M., Cellier, D., Dhanani, S., D'Esposito, M., 2020. Causal evidence for a role of theta and alpha oscillations in the control of working memory. Curr. Biol. 30 https://doi.org/10.1016/j.cub.2020.02.065, 1748-1754.e4.

Roux, F., Uhlhaas, P.J., 2014. Working memory and neural oscillations: α-γ versus θ-γ codes for distinct WM information? Trends. Cogn. Sci. 18, 16–25. https://doi.org/10.1016/j.tics.2013.10.010.

Sarnthein, J., Petsche, H., Rappelsberger, P., Shaw, G.L., von Stein, A., 1998. Synchronization between prefrontal and posterior association cortex during human working memory. Proc. Natl. Acad. Sci. u S. a 95, 7092–7096. https://doi.org/10.1073/pnas.95.12.7092.

Sauseng, P., Griesmayr, B., Freunberger, R., Klimesch, W., 2010. Control mechanisms in working memory: a possible function of EEG theta oscillations. Neurosci. Biobehav. Rev. 34, 1015–1022.

Sauseng, P., Hoppe, J., Klimesch, W., Gerloff, C., Hummel, F.C., 2007. Dissociation of sustained attention from central executive functions: local activity and interregional connectivity in the theta range. Eur. J. Neurosci. 25, 587–593. https://doi.org/10.1111/j.1460-9568.2006.05286.x.

Sauseng, P., Klimesch, W., Doppelmayr, M., Hanslmayr, S., Schabus, M., Gruber, W.R., 2004. Theta coupling in the human electroencephalogram during a working memory task. Neurosci. Lett. 354, 123–126. https://doi.org/10.1016/j.neulet.2003.10.002.

Sauseng, P., Klimesch, W., Doppelmayr, M., Pecherstorfer, T., Freunberger, R., Hanslmayr, S., 2005. EEG alpha synchronization and functional coupling during top-down processing in a working memory task. Hum. Brain Mapp. 26, 148–155. https://doi.org/10.1002/hbm.20150.

Sauseng, P., Klimesch, W., Heise, K.F., Gruber, W.R., Holz, E., Karim, A.A., Glennon, M., Gerloff, C., Birbaumer, N., Hummel, F.C., 2009. Brain oscillatory substrates of visual short-term memory capacity. Curr. Biol. 19, 1846–1852. https://doi.org/10.1016/j.cub.2009.08.062.

Scheeringa, R., Petersson, K.M., Oostenveld, R., Norris, D.G., Hagoort, P., Bastiaansen, M. C.M., 2009. Trial-by-trial coupling between EEG and BOLD identifies networks related to alpha and theta EEG power increases during working memory maintenance. Neuroimage 44, 1224–1238. https://doi.org/10.1016/j.neuroimage.2008.08.041.

Schmidt, R., Herrojo Ruiz, M., Kilavik, B.E., Lundqvist, M., Starr, P.A., Aron, A.R., 2019. Beta oscillations in working memory, executive control of movement and thought, and sensorimotor function. J. Neurosci. 39, 8231–8238. https://doi.org/10.1523/JNEUROSCI.1163-19.2019.

Sederberg, P.B., Kahana, M.J., Howard, M.W., Donner, E.J., Madsen, J.R., 2003. Theta and gamma oscillations during encoding predict subsequent recall. J. Neurosci. 23, 10809–10814. https://doi.org/10.1523/JNEUROSCI.23-34-10809.2003.

Sghirripa, S., Graetz, L., Merkin, A., Rogasch, N.C., Ridding, M.C., Semmler, J.G., Goldsworthy, M.R., 2021. The role of alpha power in the suppression of anticipated distractors during verbal working memory. Brain Topogr. 34, 102–109. https://doi.org/10.1007/s10548-020-00810-4.

Snyder, A.C., Foxe, J.J., 2010. Anticipatory attentional suppression of visual features indexed by oscillatory alpha-band power increases: a high-density electrical mapping study. J. Neurosci. 30, 4024–4032. https://doi.org/10.1523/JNEUROSCI.5684-09.2010.

Spyropoulos, G., Bosman, C.A., Fries, P., 2018. A theta rhythm in macaque visual cortex and its attentional modulation. Proc. Natl. Acad. Sci. u S. a 115, E5614–E5623. https://doi.org/10.1073/pnas.1719433115.

Tarasi, L., Magosso, E., Ricci, G., Ursino, M., Romei, V., 2021. The directionality of fronto-posterior brain connectivity is associated with the degree of individual autistic traits. Brain Sci. 11, 1443. https://doi.org/10.3390/brainsci11111443.

Toppi, J., Astolfi, L., Risetti, M., Anzolin, A., Kober, S.E., Wood, G., Mattia, D., 2017. Different topological properties of EEG-derived networks describe working memory phases as revealed by graph theoretical analysis. Front. Hum. Neurosci. 11, 637. https://doi.org/10.3389/fnhum.2017.00637.

Ursino, M., Serra, M., Tarasi, L., Ricci, G., Magosso, E., Romei, V., 2022. Bottom-up vs. top-down connectivity imbalance in individuals with high-autistic traits: An electroencephalographic study. Front. Syst. Neurosci. 16, 932128 https://doi.org/10.3389/fnsys.2022.932128.

van Diepen, R.M., Miller, L.M., Mazaheri, A., Geng, J.J., 2016. The role of alpha activity in spatial and feature-based attention. eNeuro 3. https://doi.org/10.1523/ENEURO.0204-16.2016. ENEURO.0204-16.2016.

Vissers, M.E., van Driel, J., Slagter, H.A., 2016. Proactive, but not reactive, distractor filtering relies on local modulation of alpha oscillatory activity. J. Cogn. Neurosci. 28, 1964–1979. https://doi.org/10.1162/jocn_a_01017.

Wang, C., Rajagovindan, R., Han, S.-M., Ding, M., 2016. Top-down control of visual alpha oscillations: sources of control signals and their mechanisms of action. Front. Hum. Neurosci. 10, 15. https://doi.org/10.3389/fnhum.2016.00015.

Wang, X., Chen, Y., Ding, M., 2008. Estimating Granger causality after stimulus onset: a cautionary note. Neuroimage 41, 767–776. https://doi.org/10.1016/j.neuroimage.2008.03.025.

Wianda, E., Ross, B., 2019. The roles of alpha oscillation in working memory retention. Brain Behav. 9, e01263. https://doi.org/10.1002/brb3.1263.

Womelsdorf, T., Johnston, K., Vinck, M., Everling, S., 2010. Theta-activity in anterior cingulate cortex predicts task rules and their adjustments following errors. Proc. Natl. Acad. Sci. u S. a 107, 5248–5253. https://doi.org/10.1073/pnas.0906194107.

Xie, Y., Li, Y., Duan, H., Xu, X., Zhang, W., Fang, P., 2021. Theta oscillations and source connectivity during complex audiovisual object encoding in working memory. Front. Hum. Neurosci. 15.